Theoretical and Applied Climatology (2021) 147:13–33
https://doi.org/10.1007/s00704-021-03776-w

ORIGINAL PAPER

Spatio-temporal variability of atmospheric rivers and associated atmospheric parameters in the Euro-Atlantic region

Venugopal Thandlam[1,2,3] · **Anna Rutgersson**[1,2] · **Erik Sahlee**[1]

Received: 23 April 2021 / Accepted: 7 September 2021 / Published online: 1 October 2021

Abstract
We study the spatio-temporal variability of Atmospheric Rivers (ARs) and associated integrated water vapor and atmospheric parameters over the Euro-Atlantic region using long-term reanalysis datasets. Winds, temperature, and specific humidity at different pressure levels during 1979–2018 are used to study the water vapor transport integrated between 1000 and 300 hPa (IVT300) in mapping ARs. The intensity of ARs in the North Atlantic has been increasing in recent times (2009–2018) with large decadal variability and poleward shift (~5° towards the North) in landfall during 1999–2018. Though different reanalysis datasets show similar spatial patterns of IVT300 in mapping ARs, bias in specific humidity and wind components led to IVT300 mean bias of 50 kg m^{-1} s^{-1} in different reanalysis products compared to ERA5. The magnitude of winds and specific humidity in the lower atmosphere (below 750 hPa) dominates the total column water vapor and intensity of ARs in the North Atlantic. Reanalysis datasets in the central North Atlantic show an IVT300 standard deviation of 200 kg m^{-1} s^{-1} which is around 33% of the ARs climatology (~600 kg m^{-1} s^{-1}). Though ARs have a higher frequency of landfalling over Western Europe in winter half-year, the intensity of IVT300 in winter ARs is 3% lower than the annual mean. The lower frequency of ARs in the summer half-year shows 3% higher IVT300 than the annual mean. While ARs in the North Atlantic show a strong decadal change in frequency and path, the impact of the North Atlantic Oscillation (NAO) and Scandinavian blocking on the location of landfall of ARs are significant. Furthermore, there is a strong latitudinal dependence of the source of moisture flux in the open ocean, contributing to the formation and strengthening ARs.

1 Introduction

Tropospheric atmospheric dynamics are guided by water vapor in the lower atmosphere. Particularly, heat and momentum in the lower troposphere have strong coupling with the movement of moisture in the troposphere (Schneider et al. 1999). The ocean and atmospheric general circulation play a key role in the poleward transport of heat and water vapor and their circulation in the lower troposphere. The global and continental-scale transport of water vapor has important implications for climate variability and hydrology (Brubaker et al. 1994). This includes the moisture transport in midlatitudes guiding the global atmosphere and climate dynamics in various temporal and spatial scales. The large-scale land–ocean atmospheric exchange of moisture demonstrates the coupling of the atmospheric branch of the hydrological cycle (Hack et al. 2006). Thus, it is essential to study the tropospheric moisture transport in various scales to better understand the global water cycle, synoptic weather patterns, and climate change due to enhanced evaporation in recent decades and global warming (Trenberth 2011). Hence, atmospheric scientists must consider studying climatological, meteorological, and hydrological aspects of the transport of moisture in the lower atmosphere (Gimeno 2013; Gimeno et al. 2012). In this process, it is particularly important to understand conceptual models of moisture transport to aid research into the origin of continental precipitation (Gimeno et al. 2014).

Most of the meridional water vapor transported across midlatitudes (90% of the total midlatitudes vertically integrated water vapor flux) takes place through narrow corridors in less than 10% of the zonal circumference. These narrow filaments of poleward water vapor transports are

✉ Venugopal Thandlam
venu.thandlam@geo.uu.se

[1] Department of Earth Sciences, Uppsala University, Uppsala, Sweden

[2] Centre of Natural Hazards and Disaster Science, Uppsala University, Uppsala, Sweden

[3] Centre for Environment and Development Studies (CEMUS), Uppsala University, Uppsala, Sweden

termed atmospheric rivers (ARs) (Zhu and Newell 1998; Ralph et al. 2004). These transient filamentary regions occur within the warm conveyor belt of extratropical cyclones in a maritime environment and are characterized by high water vapor content and strong low-level winds (Ralph et al. 2004, 2005, 2006). Thus, these corridors tend to be quite narrow (< 1000 km wide) relative to their length scale (> 2000 km) (Neiman et al. 2008a). The warm conveyor belt transports both sensible and latent heat, particularly the latter contributes to the poleward heat transport that occurs in the form of water vapor flux from the warm sea surface over oceanic regions serving as a major moisture source. Most of the water vapor transport within these rivers occurs in the lowest 2.5 km of the atmosphere due to moist-neutral stratification (Ralph et al. 2005). Hence, these are also called tropospheric rivers due to their occurrence in the lower troposphere (Zhu and Newell 1994, 1998). The combination of lower tropospheric moist neutrality, strong horizontal winds, large and concentrated water vapor content yields an occurrence of heavy orographic precipitation and winds on elevated terrain, which can lead to severe and widespread flooding (Ralph et al. 2006; Neiman et al. 2002, 2011; Leung and Qian 2009; Lavers et al. 2011, 2012; Waliser and Guan 2017; De Luca et al. 2017), and could further cause landslides to occur over the adjacent area (Cordeira et al. 2019). Heavy and untimely precipitation from warm ARs also causes preexisting snowpack to melt in high latitudes and poles allowing freshwater inflow into oceans and contribute to the sea level rise (Thapa 2015; Yang et al. 2018; Neff William 2018; Mattingly et al. 2018), leading to coastal flooding (Khouakhi and Villarini 2016). Snowmelt and intense flooding due to ARs could change the geomorphic processes, biodiversity, and mass mortality of wildlife (Florsheim and Dettinger 2015; Cheng et al. 2016). Conversely, ARs could also change the ice sheet surface mass balance over poles through heavy snow accumulation (Gorodetskaya et al., 2014). Thus, ARs are key to understanding extratropical and polar hydro-climate features through polar warming, sea ice melt, and precipitation (Nash et al. 2018; Komatsu et al. 2018). Consequently, these mesoscale filamentary features play a key role in the global water cycle and represent an important phenomenon linking weather and climate.

There are numerous studies over midlatitudes documenting the AR characteristics, landfall, and their relationship with the extreme hydrometeorological events (De Luca et al. 2017). Many studies have focused on ARs over the Pacific, particularly on the West coast of the United States (Ralph et al. 2005, 2006, 2019; Neiman et al. 2008a; and the references therein) and South America (Viale and Nunez 2011). There are a few studies aimed at the global characteristics of ARs (Waliser and Guan 2017; Guan and Waliser 2017, 2015). Recently, there is an increasing focus on the precipitation over Europe and ARs over the North Atlantic (Pasquier et al., 2019; Gao et al. 2016; Lavers et al. 2016; Champion et al. 2015). Recent studies in Asia (Thapa 2015; Yang et al. 2018; Kamae et al. 2017) and Africa (Blamey et al. 2018; Ramos et al. 2018) have focused on the relationship between ARs and extremes in precipitation. However, the study of ARs over the North Atlantic and Europe needs more attention due to potentially increasing extremes in hydrometeorological events such as snowfall, precipitation, and flooding (Millán 2014; Kundzewicz et al. 2006; Van den Besselaar et al. 2013; Sodemann and Stohl 2013; Stohl et al. 2008). Most of the extreme wind events catalogued between 1997 and 2013 over Europe with billion US dollar losses were associated with ARs (Waliser and Guan 2017). Hence, it is essential to study both oceanic and atmospheric processes affecting these anomalies and extremes. AR is one such feature guided by both oceanic and atmospheric dynamics and causes extremes in precipitation and influences the hydrology over Europe. Lavers and Villarini (2013b) studied the relationship between ARs and extreme precipitation across Europe and found that the North Atlantic Oscillation (NAO) has a significant impact on precipitation caused by ARs. The same study highlighted the anomalies in central European precipitation patterns caused by ARs over the North Atlantic. According to a multi-model ensemble of the Coupled Model Intercomparison Project (CMIP5), AR frequency is projected to increase 127–275% by the end of this century, at peak AR frequency regions (45°–55°N) over Europe, under the representative concentration pathway 8.5 (RCP8.5) scenario. This enhanced frequency is associated with the wind changes in the midlatitude jet (Gao et al. 2016; Espinoza et al. 2018). ARs cause 20–30% of all precipitation in parts of Europe and the USA, however with strong seasonality. Also, ARs penetrate further inland over Europe than over the USA (Lavers and Villarini 2015). Thus, ARs are in sync with the largest floods over Western Europe and the UK (Lavers et al. 2011, 2012; De Luca et al. 2017).

Several procedures are in practice to detect, track, and forecast ARs in advance using observational, reanalysis, and numerical models (Ralph et al. 2019; Fish et al. 2019; Lavers et al. 2018). Integrated water vapor (IWV) (Ralph et al. 2004; Neiman et al. 2008b; Guan et al. 2010) and integrated vapor transport (IVT) (Zhu and Newell 1998; Roberge et al. 2009; Jiang and Deng 2011) are the two most common techniques used to define, detect, and track ARs. Time integrated IVT, Meteograms, and cross-sections are some other methods to study ARs. Both IWV and IVT consider vertically integrated (between 1000 and 300 hPa or less) horizontal water vapor transport (significant poleward moisture transport) when the standardized values are greater than a threshold while mapping AR occurrence (Roberge et al. 2009). Hence, accurate atmospheric parameters such as winds, specific humidity, and the temperature at different pressure levels obtained from satellites and reanalysis

products are essential to study ARs (Neiman et al. 2009; Dettinger 2011). Though necessary parameters are available from different platforms, atmospheric reanalysis is the best estimate of the historical state of the Earth's atmosphere. These datasets are produced by assimilating meteorological/oceanic observations into numerical weather prediction model output.

In this work, we study the characteristics of ARs over the North Atlantic such as spatiotemporal variability, frequency, and decadal variability of ARs and bias in mapping ARs using different reanalysis products with respect to newly released ERA5 reanalysis data. The objective of this study is also to look at the spatial and temporal variability and trend of ARs in the North Atlantic in relation to the different atmospheric parameters, and IVT in different layers of the atmosphere using ERA5 data. The spatial/horizontal resolution dependence of ARs over the North Atlantic from different reanalysis products was computed with reference to 1000–300 hPa and compared with ERA5. We also study the state of the atmosphere and synoptic conditions during the landfalling ARs. Thus, the paper is organized as follows. Section 2 describes the data and methods, followed by results and discussions in Section 3 and conclusions in Section 4.

2 Data and methods

We have used six-hourly winds, temperature, and specific humidity data at different pressure levels from six reanalysis products available during 1979–2018. These six reanalysis datasets include 20th Century Reanalysis version 2 (20CR-V2) (Compo et al. 2011) from the NOAA Earth System Research Laboratories (ESRL), ERA-Interim (Dee et al. 2011), ERA5 (Hersbach et al. 2017) from the European Centre for Medium-Range Weather Forecasts (ECMWF), Modern-Era Retrospective analysis for Research and Applications (MERRA-2) (Gelaro et al. 2017) from National Aeronautics and Space Administration (NASA), Climate Forecast System Reanalysis version 2 (CFSR-v2) (Saha et al. 2014), and NCEP-NCAR Reanalysis version 2 (Kanamitsu et al. 2002) from the National Center for Environmental Prediction (NCEP). Apart from MERRA-2, which has been available since 1980, all datasets are available from 1979 and have different spatial resolutions. Details of reanalysis datasets are given in Table 1.

In addition to traditionally mapping ARs using both IVT (Eq. (2)) and IWV (Eq. (4)), we also used the temperature of corresponding layers in these methods to normalize the computed IVT (nIVT, Eq. (3)) and IWV (nIWV, Eq. (5)) and study the difference from the normal approach using different reanalysis products and compared these two methods in the North Atlantic using ERA5 data. Temperature normalization is done to understand the change in the thermodynamic component of IVT and IWV using the Clausius–Clapeyron Eq. (1), which states that the water–vapor content of saturated air, q*, increases nearly exponentially with temperature T (Payne et al. 2020).

$$\frac{dq^*}{dT} = \alpha(T)q^* \tag{1}$$

α(T) is the Clausius-Clapeyron scaling factor, defined as

$$\alpha(T) = \frac{L}{R_v T^2}$$

where L is the latent heat of vaporization and R_v is the gas constant of water vapor. Within the saturated environment at the core of an AR where $q \approx q*$, a small change in the surface warming would cause specific humidity to further increase.

Table 1 Details of reanalysis datasets used in the present study

Dataset	Source	Availability	Temporal resolution	Spatial resolution	Reference
20th Century Reanalysis (20CR-V2)	ESRL: PSD/NOAA	1851–2014	6 hourly	2×2×24, 1000—10 hPa	Compo et al. (2011)
ERA-Interim	ECMWF	1979–2018	6 hourly	0.75×0.75×60, 1000—0.1 hPa	Dee et al. (2011)
ERA5	ECMWF	1979–present	6 hourly	0.25×0.25×37 1000—1 hPa	Hersbach et al. (2017)
Modern-Era Retrospective analysis for Research and Applications (MERRA-2)	Global Modelling and Assimilation Office (NASA)	1980–present	6 hourly	0.5×0.625×42 1000—1 hPa	Gelaro et al. (2017)
Climate Forecast System Reanalysis (CFSR-v2)	National Centers for Environmental Prediction (NCEP)	1979–present	6 hourly	0.5×0.5×64, 1000-0.266 hPa	Saha et al. (2014)
NCEP-NCAR Reanalysis—v2	NCEP-NCAR	1979–present	6 hourly	2.5×2.5×28 1000—3 hPa	Kanamitsu et al. (2002)

Thus, specific humidity in the upper layers of the atmosphere strongly depends on the increase in layer's temperature due to increased surface temperature and the Clausius-Clapeyron scaling factor, α(T) and is approximately 6.6% K^{-1} for surface temperatures causing ARs that are land-falling over California in the present climate (T = 13 °C) (Dettinger 2011; Gonzales et al. 2019).

Integrated vapor transport (IVT):

$$IVT = g^{-1}\sqrt{\left(\int_{1000}^{p} QU\,dp\right)^2+\left(\int_{1000}^{p} QV\,dp\right)^2} \quad (2)$$

Normalized IVT:

$$\mathrm{nIVT} = g^{-1}\sqrt{\left(\int_{1000}^{p} \frac{QU}{T}\,dp\right)^2+\left(\int_{1000}^{p} \frac{QV}{T}\,dp\right)^2} \quad (3)$$

Integrated water vapor (IWV):

$$IWV = g^{-1}\int_{1000}^{p} Q\,dp \quad (4)$$

Normalized IWV:

$$nIWV = g^{-1}\int_{1000}^{p} \frac{Q}{T}\,dp \quad (5)$$

where Q is specific humidity in kg kg^{-1}, U and V are zonal and meridional components of winds at different pressure levels measured in m s^{-1}, P is the desired pressure (hPa) up to which the atmospheric parameters are integrated; g is the acceleration due to gravity, which is a constant and is given as 9.8 m s^{-2} (Neiman et al. 2008a; Lavers and Villarini 2013a, 2013b). Normalization with temperature is done by dividing Q, U, and V with the temperature at a corresponding pressure level. Supplementary Table S1 shows the details of the variables and their units. Thus, six-hourly (00, 06, 12, and 18) ARs data has been generated from six-hourly reanalysis datasets using IVT (kg m^{-1} s^{-1}), normalized IVT (kg m^{-1} s^{-1} K^{-1}); IWV (mm) and normalized IWV (mm K^{-1}) from the surface to 750 hPa, 500 hPa, and 300 hPa. Shields et al. (2018) compiled all available methods including thresholds to map ARs globally as a part of describing the Atmospheric River Tracking Method Intercomparison Project (ARTMIP). These methods vary in using both spatial and temporal threshold scales for AR detection. Hence, we use the Toolkit for Extreme Climate Analysis (TECA) Bayesian AR Detection (BARD) method (O'Brien et al. 2020) to map ARs to minimize the human prejudice on the selecting and setting the threshold for different parameters to map ARs. Furthermore, quantification of ARs over the North Atlantic was done using the climatology and standard deviation in different methods. This is essential to see the spatial variability including the magnitude of water vapor transport over the North Atlantic and into Western Europe.

The 6-hourly (00, 06, 12, and 18) AR data has been used in further analysis to study temporal and spatial variability of ARs over the North Atlantic, both in climatic and decadal timescales. In addition to studying biases in different atmospheric parameters, the annual and seasonal climatology and strength of ARs at different layers were studied. For the intercomparing of reanalysis datasets, we consider ERA5 as the reference dataset because of its enhancements in parameterization and resolution. Furthermore, the study focuses on the variability of ARs intensities in different products, including major categories of ARs and their frequencies in the North Atlantic. Linear regression analysis with Student *t*-test done in the study helps to understand the spatial trend in the IVT300 (ARs), followed by the study to understand the state of the atmosphere using atmospheric parameters to describe the characteristics of land-falling of ARs.

A general approach used to map ARs is using IVT300 by considering pressure levels from surface (1000 hPa) to 300 hPa (Neiman et al. 2008b; Guan et al. 2010; Lavers et al. 2011). A few studies also considered 900 hPa as the surface reference level (Gorodetskaya et al. 2014); 500 hPa (Gao et al. 2016) and 200 hPa (Sellars et al. 2017; Mattingly et al. 2018) as upper limits. Hence, there is persisting ambiguity in using reference pressure levels to map ARs. Therefore, here we quantify the magnitude of annual and semi-annual IVT in different layers. For this purpose, the total column (1000–300 hPa) was divided into sub-layers consisting of 500–300 hPa (IVT_Upper), 750–300 hPa (IVT_Middle), 750–500 (IVT_Lower), besides computing IVT500 (1000–500 hPa) and IVT750 (1000–750 hPa). This exercise helps to map the strength of IVT and spatial variability in these layers, which is a function of exponentially decreasing water vapor pressure with height.

3 Results and discussions

3.1 ARs in the North Atlantic in ERA5

The annual climatology from ERA5 data using IVT and nIVT methods shows the highest AR intensity in the region enclosed between 30 and 60°N (Fig. 1). Though the intensity of AR varies from event to event, the mean IVT300 (IVT between 1000 and 300 hPa) (Fig. 1a) over the North Atlantic is around 600 kg m^{-1} s^{-1} and is in line and directed along the westerly wind over this region. The maximum nIVT300 (nIVT between 1000 and 300 hPa) over the North Atlantic is in coherence with the maximum IVT300 and along the same path with maximum values (> 1 kg m^{-1} s^{-1} K^{-1}) concentrated over the central North Atlantic (Fig. 1b).

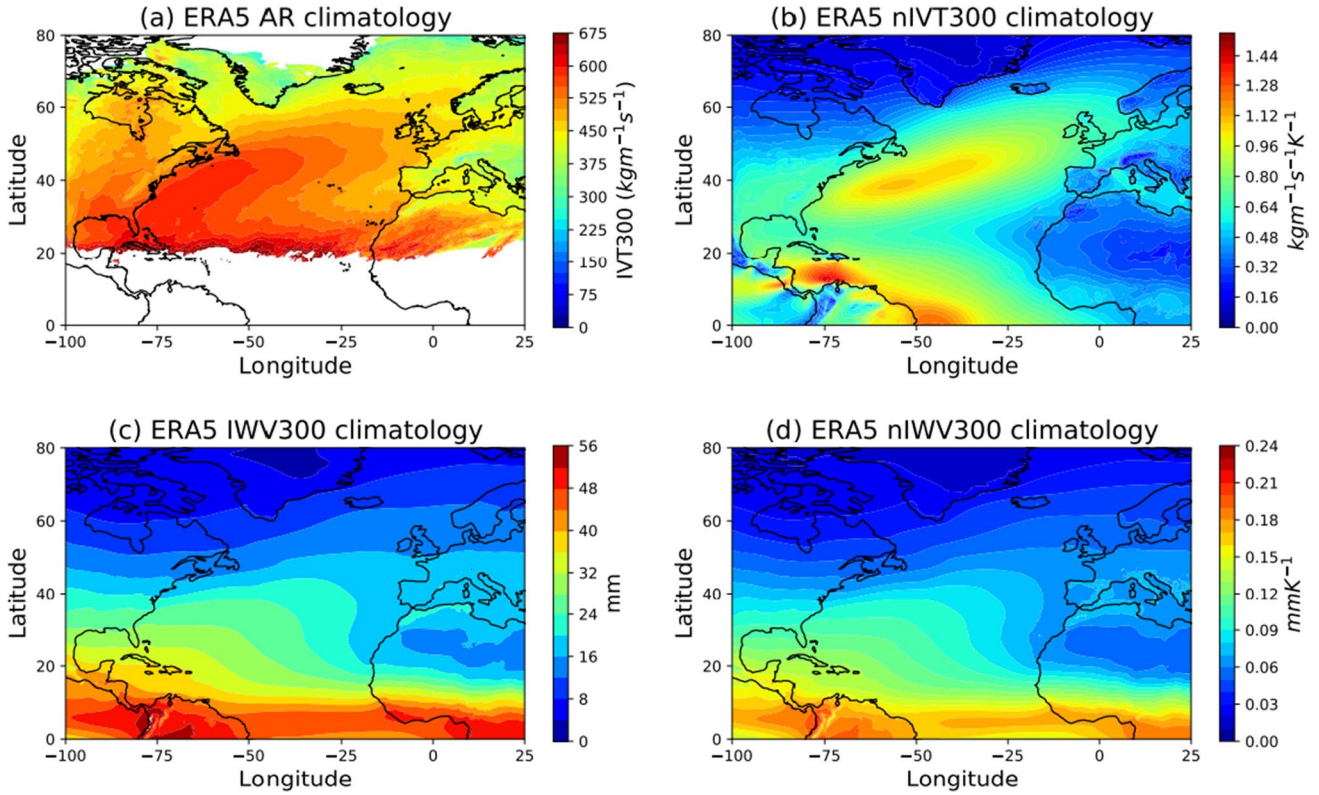

Fig. 1 Climatology of (**a**) IVT300, (**b**) nIVT300, (**c**) IWV300, and (**d**) nIWV300 computed from daily ERA5 data in the North Atlantic

The nIVT300 is accounted for available IVT300 per unit temperature, is a proxy to fractional changes in available specific humidity in the atmospheric column per degree of atmospheric warming. In the upper layers of the atmosphere, α varies with the varying temperature. Hence, α increases with the decreasing temperature with height and amplifies changes in the specific humidity aloft and is larger in the upper troposphere. On the other hand, increasing specific humidity in upper layers tends to release more latent heat flux with ascending air, and decrease the lapse rate with warming and thus increasing the temperature with height. If the vertical column of the atmosphere is saturated and has moist-neutral conditions, the combination of these factors implies a rate increase in IVT that is substantially larger than that of near-surface water vapor (Payne et al. 2020). Hence, a fractional change in IVT is a reasonable approximation to the thermodynamic contribution to IVT change. Thus, on top of concentrated warm coastal surface waters due to Gulf stream over western North Atlantic causing higher evaporation over this region, specific humidity advection from tropics could be saturating the upper troposphere over the central North Atlantic and shows high IVT300 and nIVT300.

Though AR mapping and characteristics study initially was started using IWV, the importance of tracking the AR made IVT a widely used method. However, using IWV would give an estimation of the concentration of total column condensable water vapor at a given instance (Ralph and Dettinger 2011; Gimeno et al. 2014). Climatology of IWV300 (IWV between 1000 and 300 hPa) (Fig. 1c) and nIWV300 (nIWV between 1000 and 300 hPa) (Fig. 1d) shows the gradient of water vapor varying from a maximum at the equator and fading towards the pole. Using nIWV here shows the amount of total column condensable water vapor per degree Kelvin. The amount of evaporation caused by solar heating and the strength of the near-surface winds determines the extent and the scale of the water vapor. However, the occurrence of AR over a region and its magnitude guided by the amount of precipitable water vapor are not only bound to the availability of specific humidity in the atmosphere but also to the magnitude and direction of winds carrying the water vapor. Hence, the higher intensity of ARs over the North Atlantic and Western Europe is in the direct vicinity of the region of occurrence of extratropical cyclones and associated strong surface wind speeds (Pinto et al. 2013; De Luca et al. 2017) and along the path of the subtropical westerly winds. Although all methods used in mapping ARs show higher values over the western North Atlantic, the origin of ARs and the region of moisture flux into ARs in this part of the ocean are still debatable. These elongated features are also affected by the synoptic weather conditions,

and their magnitude depends on the midway convergence of water vapor flux from adjacent areas. Despite AR climatology showing a mean IVT300 of 600 kg m^{-1} s^{-1}, each AR could be different in magnitude and its strength may vary as per the state of the atmosphere at a given instance.

One example of an AR from 6th March 2002 mapped using four different methods in Fig. 2 has IVT300 higher than 800 kg m^{-1} s^{-1} (Fig. 2a). This event was one of the intense ARs that occurred over northern Europe and caused excess rainfall over Britain and southern Scandinavia. While the IVT300 in this AR is narrow and short, nIVT300 (Fig. 2b) shows the adjacent regions saturated with water vapor. The advected moisture from these surrounding regions could enhance the intensity and lifetime of the AR over a given location. Thus, nIVT300 is a useful approach in addition to existing methods in mapping the true characteristics and saturated water vapor content in ARs. Similarly, IWV300 and nIWV300 (Fig. 2c,d) for this event show the origin of AR and the source of the advection, which, in this case, occurred from the warm tropical region (20°N) enriched with high specific humidity.

3.2 Intensity and bias of ARs in reanalysis data

Different reanalysis products used to map the ARs show large variability in magnitudes in the North Atlantic (Fig. 3). The climatology (shaded) and standard deviation (contours) of ERA5 (Fig. 3a) have lower IVT300 intensity than any other reanalysis products used, while ERA-Interim has higher climatology (intensity) and standard deviation. The highest variability (standard deviation of 200 kg m^{-1} s^{-1}) is around 33% of climatology (~600 kg m^{-1} s^{-1}) in reanalysis datasets. Both climatology and standard deviation of ARs and associated IVT300 are high in JJA and SON, and low in MAM, thus show strong seasonal variability in ERA5 (Supplementary Figure S1 and S2, respectively), and all reanalysis products show similar annual climatology and standard deviation (Fig. 3a-f). Although these values vary with seasons in different reanalysis datasets, JJA, SON, and DJF have longer stretch/extent of higher climatology and standard deviation values of ARs and IVT300 in the North Atlantic in ERA5 (Supplementary S1 and S2). Similarly, both these values have a large spread and reach Western

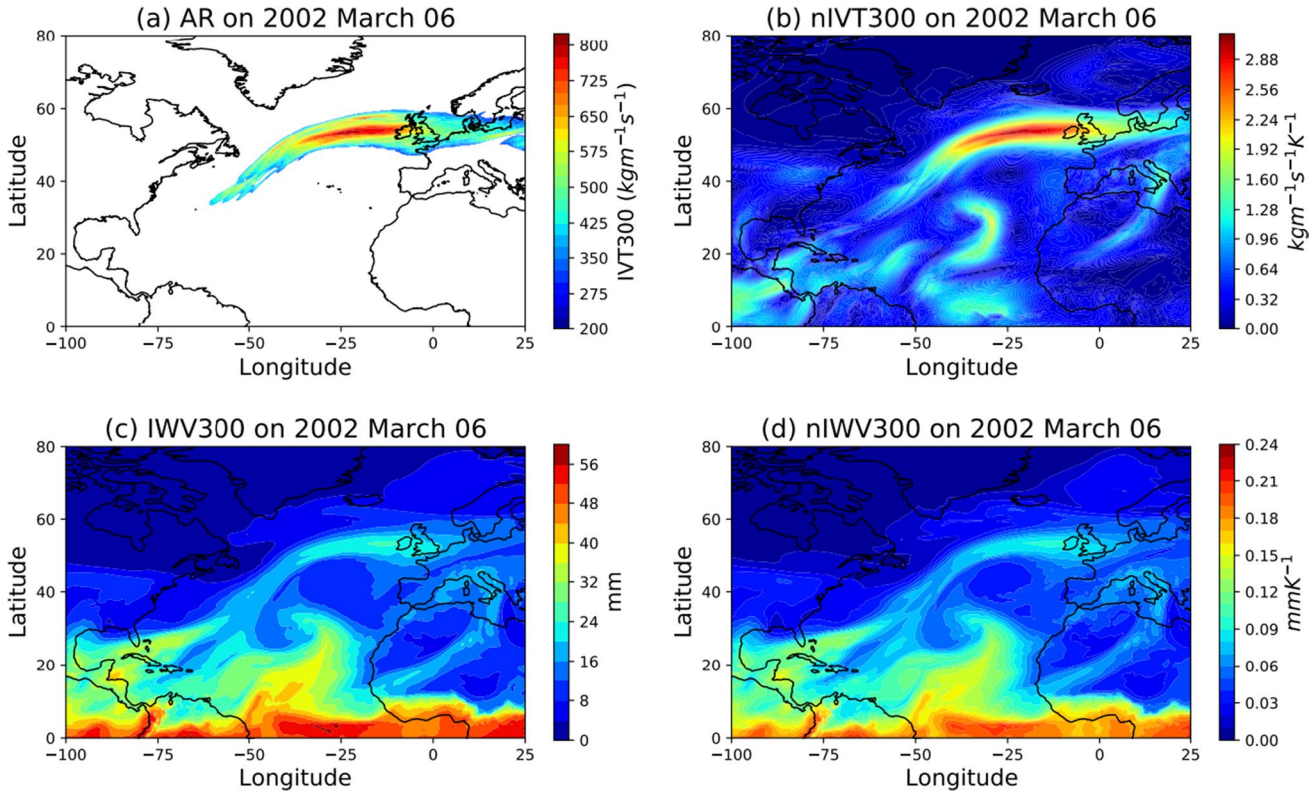

Fig. 2 AR event on 2002 March 06 mapped using four different methods in the North Atlantic using ERA5 data

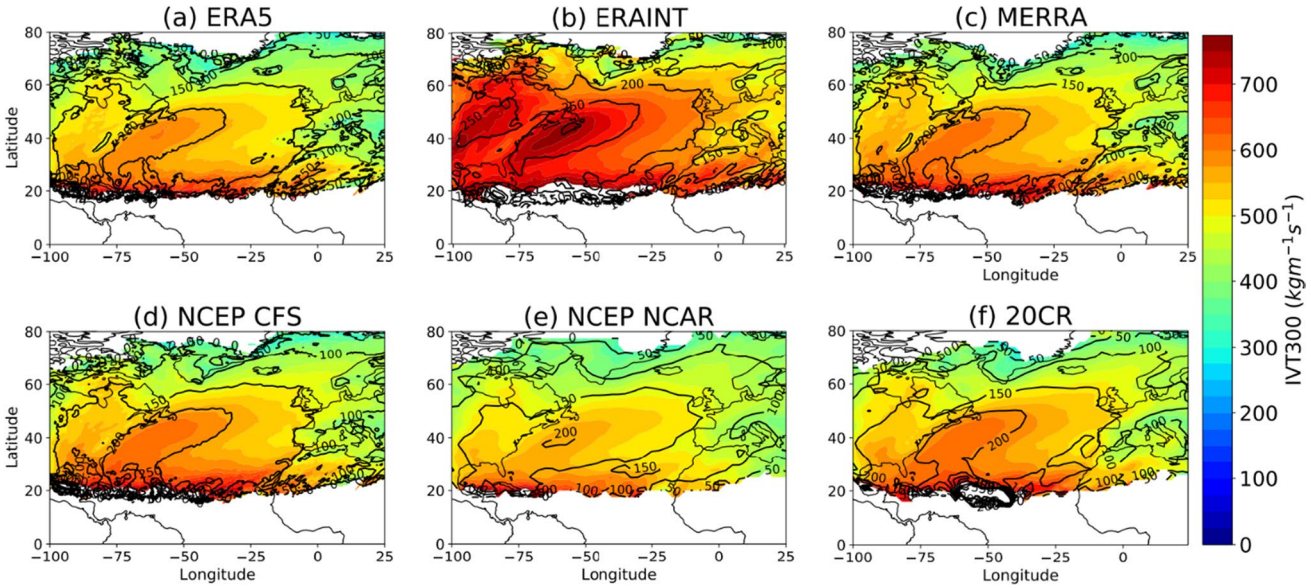

Fig. 3 Climatology (colored areas) and standard deviation (black contours) of IVT300 in the North Atlantic from all reanalysis data used in the study

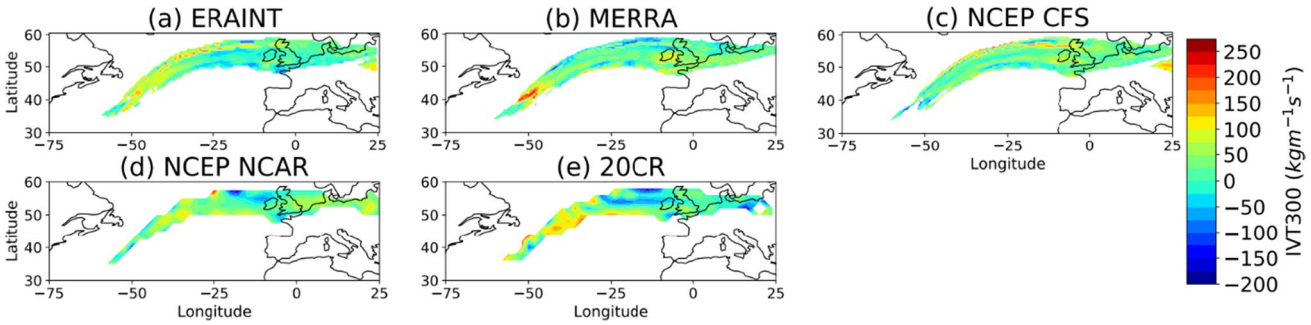

Fig. 4 Bias in reanalysis products compared to ERA5 data in mapping AR on 2002 March 06 using BARD method

Europe in winter half-year (ONDJFM), leading to a high frequency of ARs during this period (Lavers et al. 2011, 2012). Low frequency in summer half-year (AMJJAS) mainly concentrated over the central North Atlantic and shows large standard deviation.

In the case of AR mapped on 6th March 2002, different reanalysis products show significant bias in IVT300 compared to ERA5 (Reanalysis product – ERA5) (Fig. 4). Both MERRA and ERA-Interim show negative bias at the head of the AR and positive bias in the tail (Fig. 4a,b). On the other hand, NCEP (NCAR, CFS) and 20CR have a strong positive bias on aggregate (Fig. 4c-e). In this case, both these positive and negative biases are around 50 kg m^{-1} s^{-1} in magnitude and are 10% of the mean magnitude of AR (~ 500 kg m^{-1} s^{-1}) (Fig. 2). While ERA-Interim shows a larger bias of 250 kg m^{-1} s^{-1} (Supplementary Figure S3a), the total bias in the ARs mapped using other reanalysis products with respect to ERA5 during 1979–2018 vary from – 70 to 70 kg m^{-1} s^{-1} in the North Atlantic (supplementary Figure S3b-S3e). Thus, the variability in the magnitude of ARs in different products might lead to bias in the intensity, estimation of precipitation and winds during landfall. Hence, we use ERA5 data as a standard dataset in our further analysis in the following sections.

All reanalysis data sets are developed using numerical and statistical approaches integrated with observations and possible bias corrections. Thus, all the reanalysis datasets show a similar spatial pattern over the North Atlantic, but the difference in magnitudes is explained by the variability in the magnitudes of Q, U, and V, which could be further due to bias in observations, and discrepancies in product development. To illustrate it further, we compared the atmospheric parameters used (Q, U, and V) to map AR in 20CR (coarse resolution) with the ERA5 (high-resolution data) (Figure S4). A simple interpolation is used to match grid points of parameters in

ERA5 with 20CR data as these data sets have a different spatial resolution. The climatology of these individual parameters during 1979–2014 shows that 20CR overestimates (ERA5-20CR) the magnitude (Figures S4d-S4f) compared to the ERA5 (Figures S4a-S4c). Hence, the 20CR data has a bias of 0.5 g kg^{-1} in Q, 1 m s^{-1} in U and V components of wind in the North Atlantic (Figures S4g-S4i) compared to ERA5. However, this would not be obvious for different seasons and different ARs in the North Atlantic due to strong seasonal variability of IVT300 intensities and atmospheric state which makes each AR unique event.

3.3 Spatiotemporal variability of IVT in the North Atlantic

The annual, winter half-year and summer half-year mean IVT computed using ERA5 data in IVT_Upper, IVT_Middle and IVT_Lower are shown in the supplementary Figure S5. Due to low saturated water vapor in the higher altitudes, IVT_Upper in the North Atlantic has a lower magnitude (~20 kg m^{-1} s^{-1}) as compared to IVT_Middle (> 80 kg m^{-1} s^{-1}) and IVT_Lower (~70 kg m^{-1} s^{-1}) in the half years. Though the magnitude is less, winds in the IVT_Upper play a key role in guiding these narrow filaments of ARs poleward. As the IVT_Middle (750–300 hPa) includes IVT_Upper (500–300 hPa), the total IVT in the 750–500 hPa layer is ~60 kg m^{-1} s^{-1}. When separating these pressure levels, IVT shows a dipole pattern with a low below 20° N over the northwestern African coast and a high in the central North Atlantic extending from 30° N to 60° N. The green rectangular box in Figure S5b shows the region with maximum IVT (30° N–60° N, 80° W–0). The magnitude of high in the dipole is further increased during the summer half-year in all layers (Figure S5g-S5i). Similarly, the low has become further less during the winter half-year (Figure S5d-S5f). Thus, IVT has maximum strength during the summer half-year which could be due to strong evaporation over the warm waters in the North Atlantic.

Figure 5 shows the strength of annual, summer half-year and winter half-year mean IVT in the central North Atlantic (30° N–60° N, 80° W–0) computed from ERA5 data using different reference pressure levels at the top (300 hPa, 500 hPa, and 750 hPa) with respect to 1000 hPa. No significant difference was seen between IVT500 and IVT300 (~ 12 kg m^{-1} s^{-1}) during the study period. But IVT750 contributed ¾ of the total strength of IVT300 and IVT500. Thus, the strength of the IVT300 and IVT500 depends on the near-surface processes below 750 hPa. While the strength of the IVT in the individual layers shows no large changes with seasons, IVT in summer half-year has a 3% higher magnitude, and IVT in the winter half-year shows a 3% lower magnitude compared to the annual mean (Fig. 5). The potential reason for the difference in IVT between the two half-years could be due to changes in the strength of Q, U, and V contributing to IVT. Though most ARs originate from the saturated warm tropical region, evaporation from warm waters over the east coast of North America and adjacent regions coupled with heat and turbulent flux exchange between ocean and atmosphere strengthens the magnitude of IVT in the north Atlantic ARs during their lifetime over the open ocean. Thus, warm waters with higher SSTs in the summer half-year potentially favor large evaporation and the moist neutral atmosphere above 500 hPa in the north Atlantic. Similarly, in the winter half-year, north of 30° N holds cold waters with lower SSTs and thus lead to less evaporation and moisture flux into the higher layers of atmosphere than in summer half-year. Hence, while the mean IVT

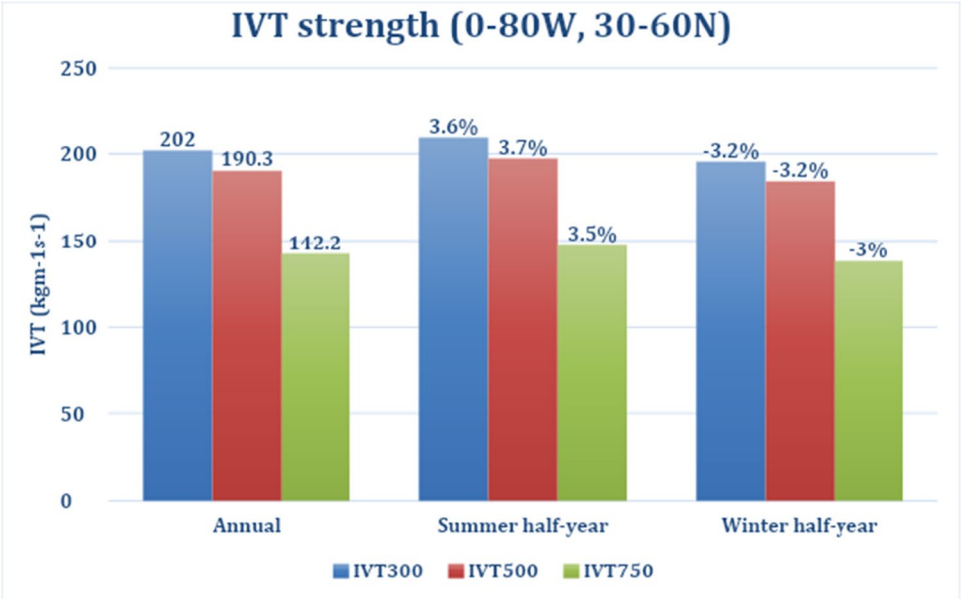

Fig. 5 Strength of annual, summer half-year and winter half-year mean IVT (kg m^{-1} s^{-1}) in different layers

is high in the below 500 hPa of the atmosphere irrespective of the season, the difference in evaporation and saturation of upper atmosphere above 500 hPa could lead to the seasonal changes in the magnitude of IVT in this region. On the other hand, the seasonal changes in the U and V guide the frequency of ARs landfalling in the North Atlantic and are discussed in the subsequent sections. Thus, improved parameterization, in addition to accurate and high-resolution atmospheric data, at least up to 500 hPa would be handy in better estimating the strength of the IVT in the North Atlantic.

Furthermore, we show a Hovmöller diagram of the monthly IVT300 (Fig. 6a) and ARs (Fig. 6b) in the central North Atlantic averaged between 30° N and 60° N along 80° W-0 during 2014–2018 to study the seasonal variability of ARs and associated IVT300 in more detail. IVT300 peaks in the western North Atlantic (along the east coast of North America) during the summer months. Due to large temperature and pressure gradients from south to north coupled with extratropical cyclone season, high IVT300 has been shifting towards the eastern North Atlantic in winter (Fig. 6a) and thus causing frequent ARs landfall over Western Europe during winter half-year. Yet, the extent, location, and movement of the ARs were not constant and have large interannual variability with relatively low values during the spring season and hence the low AR activity during this period (Fig. 6b). This interannual and intraseasonal variability in IVT300 could be caused by the altering winds (both zonal and meridional components) in the form of changes in their magnitude and direction over this region as discussed and shown in the following sections. Further, we explored the decadal variability and trend in IVT300 and related atmospheric components in the following section to study IVT variability and causes for the same in relation to associated atmospheric parameters during the study period (1979–2018).

3.4 Variability and trend of ARs and IVT300

It is evident that recent climate change caused global warming altered the global water cycle. On this note, it is important to look for changes in the ARs and IVT variability and trend in the past decades. Due to warming surface and enhanced evaporation, the changing Clausius-Clapeyron scaling factor α(T) could increase the total water vapor content in the individual atmospheric layers. The decadal trend and variability of ARs in the central North Atlantic is shown in Fig. 7. The results show an increase in the annual trend of IVT300 monthly anomaly in ARs (black line) over the decades in this region with significant seasonal and interannual variability. Though the overall trend shows an increasing IVT300 anomaly over this region with 2335 kg m^{-1} $year^{-1}$ in the study period, the decadal trend

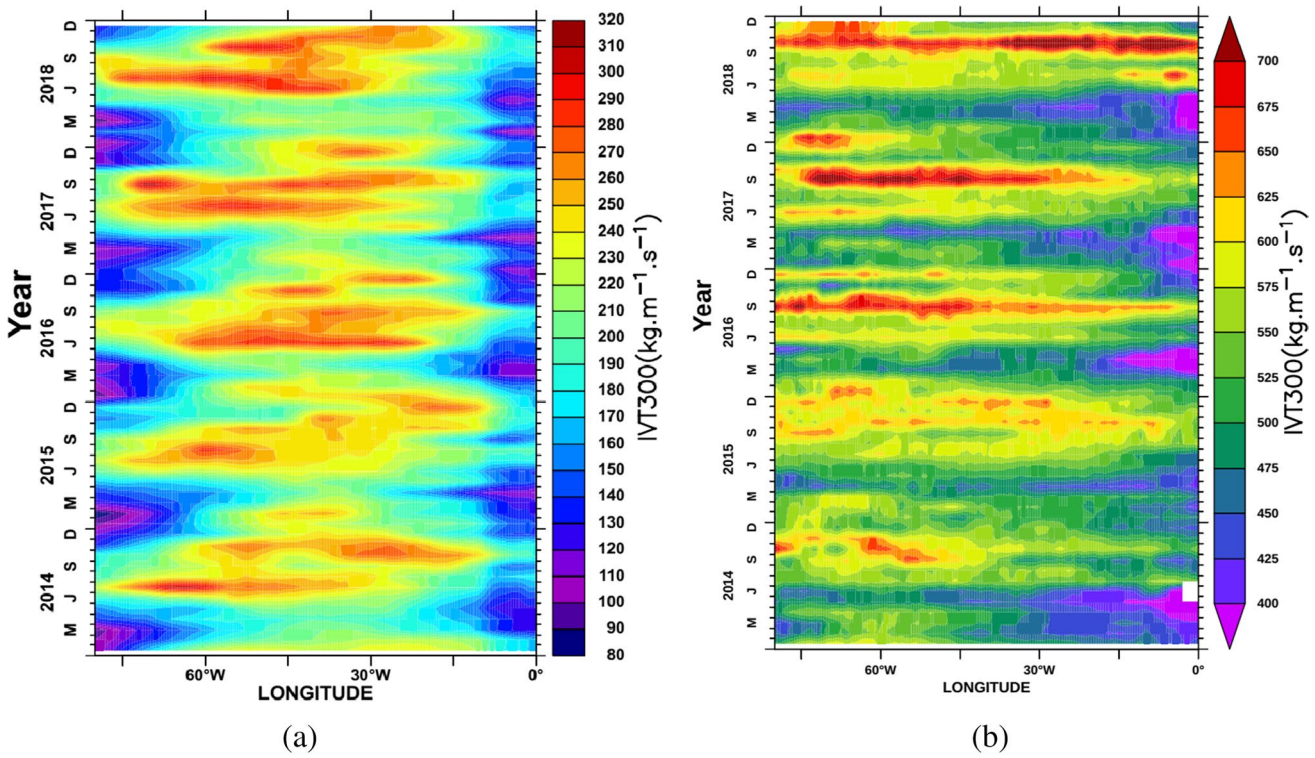

Fig. 6 (**a**) IVT300 and (**b**) AR monthly variability averaged over 30° N–60° N along 80° W–0 during 2014–2018

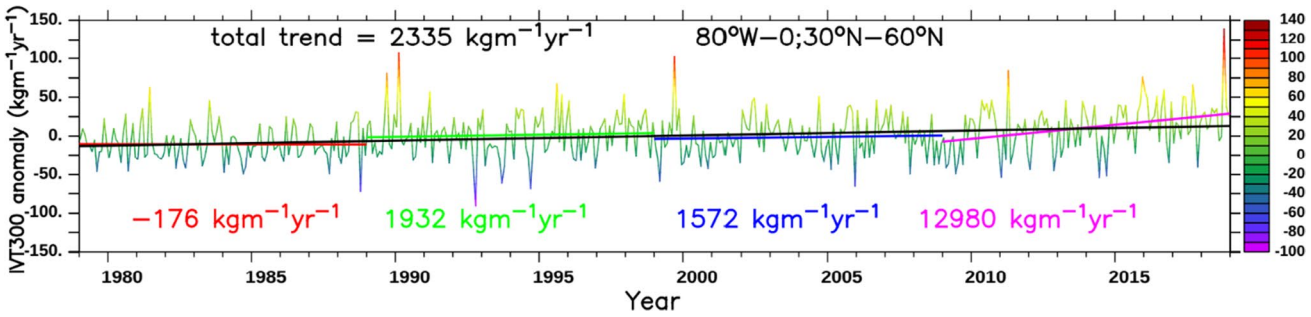

Fig. 7 Interannual variability (see saw line) overlayed with decadal (red, green, blue, and purple lines) and overall trend (black line) (significant at 95%) of IVT300 anomaly of ARs averaged in the central North Atlantic (30° N–60° N, 80° W–0)

has seesaw oscillations. Negative annual IVT300 anomaly trend (− 176 kg m^{-1} year^{-1}) in the first decade, i.e., 1979–1988 (red) was increased to 1932 kg m^{-1} year^{-1} in the second decade (green) (1989–1998). Similarly, a large increase in the annual IVT300 anomaly in the recent decade (purple) with 12,980 kg m^{-1} year^{-1} (2009–2018) dominates the previous decade (blue) with a moderate annual increase of 1572 kg m^{-1} year^{-1} (1999–2008).

Similarly, IVT of different atmospheric layers and its dependency on variable atmospheric parameters using ERA5 data is shown in Fig. 8. For this purpose, we used the same region in the central North Atlantic (30° N–60° N, 80° W–0). The increase in the annual IVT300 trend in each decade is in coherence with the increase in IVT below 500 hPa (Fig. 8a). Particularly IVT750 has contributed more to the large increase in the second (1989–1998) and fourth decades (2009–2018). As the IVT is proportional to Q, U, and V, changes in these parameters could impact these trends. Thus, the large trend of IVT300 in the second decade is dominated by the availability of Q in the near-surface layer (1000–750 hPa) which has an annual increase of 2.5 g kg^{-1} and is the largest in all decades (Fig. 8b). On the other hand, Q in the middle and upper atmosphere has been increasing with time. This increase in humidity in the upper atmosphere could be due to warming atmospheric layers which could increase the moisture-holding capacity of the air as shown in Eq. (1). Similarly, the moisture uptake from the open oceans also increased in recent times, thus fueling the flux into the upper atmosphere. Hence, significant increase of global anomalous moisture uptake feeding landfalling ARs in recent times (Algara et al. 2020). However, the negative trend in the zonal and meridional components of wind (Fig. 8c,d) in all layers during the same period guides the total trend in the second decade. Thus, while an increase in specific humidity in the lower troposphere was high in the second decade, weak zonal winds during the same period led to lower IVT over this region than in the fourth decade. Whereas, in the fourth decade strong specific humidity was equally favored by strong zonal and meridional components of the wind in the region and led to higher IVT. Similarly, while Q has a positive trend in the first and third decade, the negative trend in wind components during the same period in different layers caused the IVT annual tend to be moderate in these decades. Thus, the annual trend of both Q and wind components (U and V) were positive in the fourth decade (Fig. 8b,c,d) and led to a large increase in the annual IVT in all layers (Fig. 8a). Though the mean IVT flow is zonal, in the last two decades, the meridional wind shows a positive trend (Fig. 8d), which could have increased the flow towards the north and drove ARs poleward. Hence, the mutual coherence of magnitudes and variability of both specific humidity and wind components over the north Atlantic could guide the magnitude of IVT and ARs strength over the region.

The spatial trend analysis is significant at 95% during annual, winter half-year and summer half-year using IVT300 data from ERA5 is shown in Fig. 9. While the annual trend shows a rapid increase (3000 kg m^{-1} year^{-1}) of IVT300 at 20° N in the western North Atlantic extended into central North Atlantic with a mean annual IVT300 increase of 2000 kg m^{-1} year^{-1}, there was no significant increase in IVT300 over southwestern Europe during the study period (Fig. 9c). There are seasonal differences in which both winter half-year and summer half-year show opposite spatial trends. IVT300 increase in the central North Atlantic and the southwestern United Kingdom during the summer half-year could be triggered by the large IVT300 available over the western North Atlantic during this time (Fig. 9b, Fig. 6). Though the Winter half-year shows opposite patterns with a negative trend in IVT300, the low is over the northern United Kingdom. There was a moderate increase in the IVT300 trend along with southwestern Europe and the region below 20° N had a large positive trend during the winter half-year (Fig. 9a). IVT300 has been increasing poleward in recent times with a strong positive trend along 45° W during all seasons, which could lead to intense ARs moving towards the north.

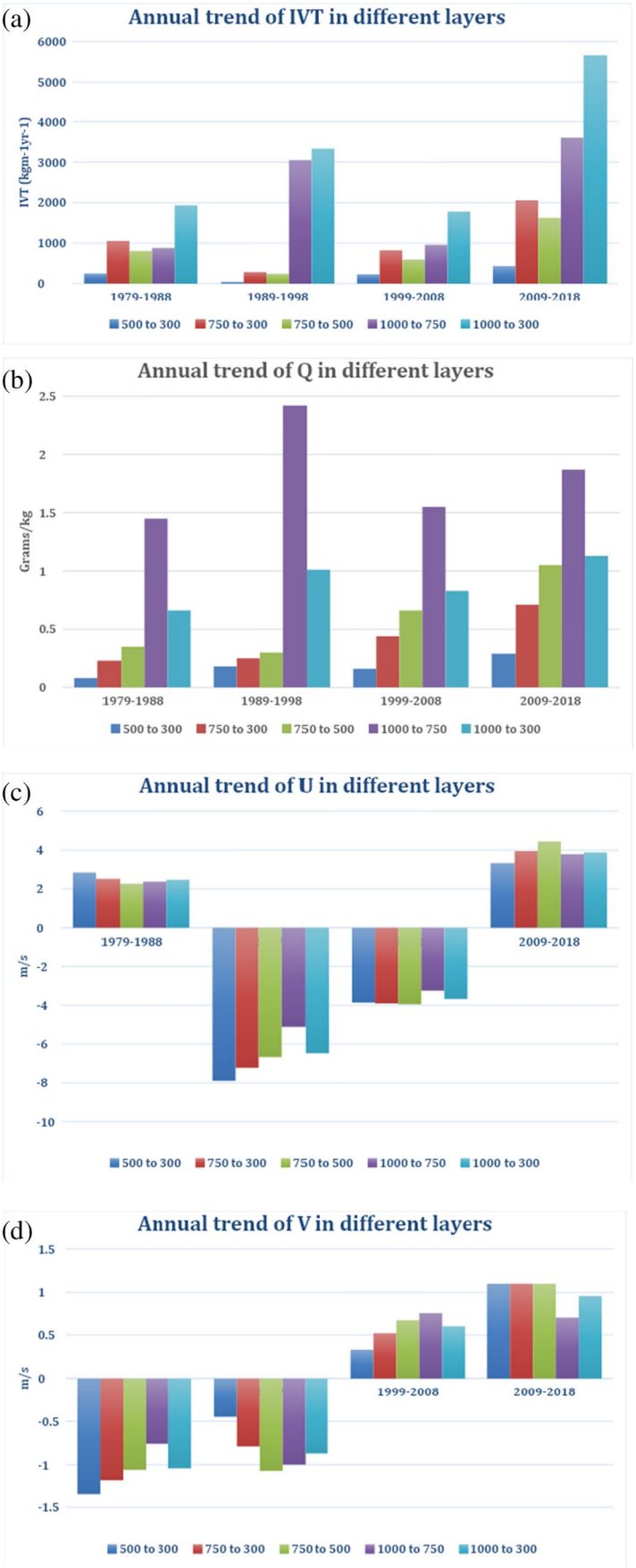

Fig. 8 Decadal trend (significant at 95%) and variability of (**a**) IVT, (**b**) specific humidity, (**c**) zonal wind, and (**d**) meridional wind of different layers in the central North Atlantic (30° N–60° N, 80° W–0)

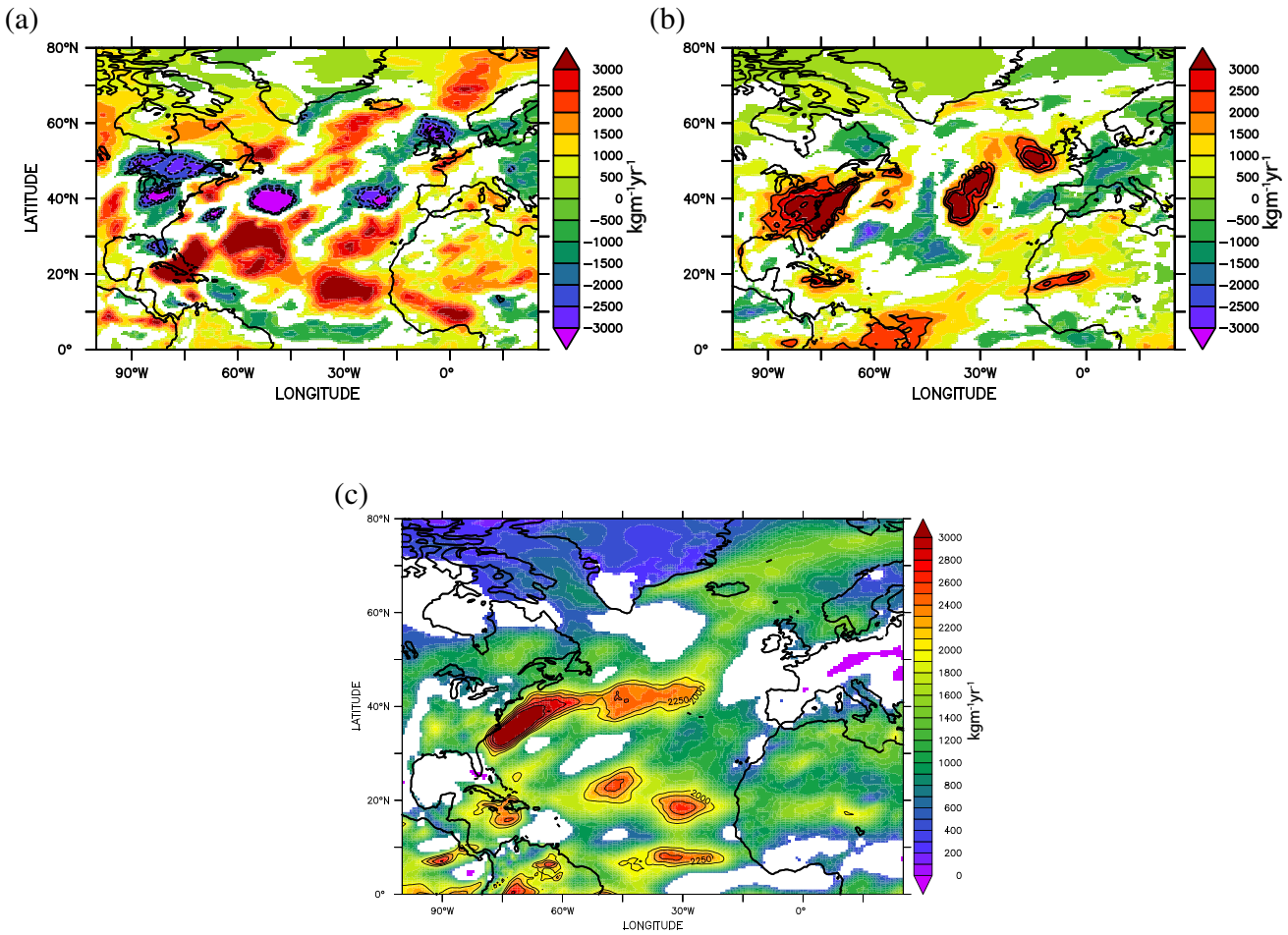

Fig. 9 Spatial trend analysis of IVT300 during (**a**) winter half-year, (**b**) summer half-year, and (**c**) annual (at 95% significance). White areas indicate no significant trend

Table 2 Categories of IVT300 based on intensity

S. No	Category	Threshold (kg m^{-1} s^{-1})
1	Cat 1	$200 \leq IVT300 < 500$
2	Cat 2	$500 \leq IVT300 < 750$
3	Cat 3	$750 \leq IVT300 < 1000$
4	Cat 4	$IVT300 \geq 1000$

3.5 Categories and frequency of ARs over the North Atlantic

The spatial variability of frequency of ARs over the North Atlantic using different categories of ARs based on the IVT300 magnitude at each grid point is shown in Table 2. We distinguish the ARs (IVT300) based on Ralph et al. (2019) with some minor changes to the thresholds, but only using the magnitude of the intensity at each grid point or location in the selected region without considering the duration of the event. The spatial frequency was computed using the percentage of the ratio of the number of days of ARs (IVT300) of the specific category to the total number of timesteps in the study period. Thus, cat 1 and cat 2 events are more frequent in the North Atlantic which occurs at 10% of the time (Fig. 10a,b) along the southwest coast of Europe and in the central North Atlantic. Other categories (cat 3 and cat 4) events are less frequent (< 5% of the time) over the Euro-Atlantic region (Fig. 10c–d). The humidity source of this intense IVT300 is along the western North Atlantic and a few events are reaching the west coast of Europe. Thus, the frequency of intense ARs over Europe is less with cat 3 being at 5%, and cat 4 at below 1% of the time. Nonetheless, the rare intense events which occur at less than 1% of the time potentially cause large damage over coastal areas. To investigate the same along with Western Europe, we draw the frequency histogram (Fig. 11a) and compute the probability density function (Fig. 11b) along 11° W as a gateway to Western Europe. This is different compared to Lavers and Villarini (2013b) who considered 10° W as the reference longitude

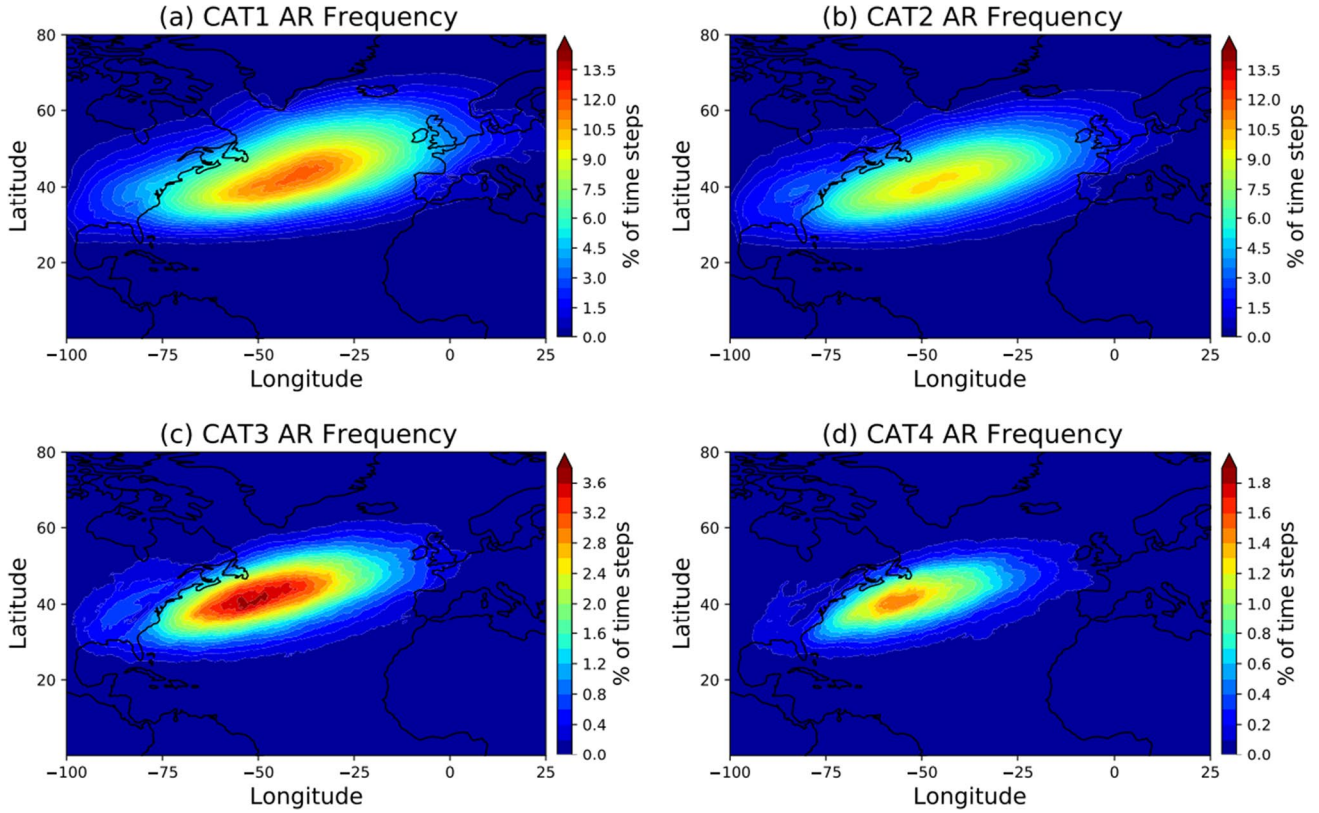

Fig. 10 Frequency of different categories of ARs in the North Atlantic

which intersects with some parts of the land over the UK and using selected events. Thus, we assume 11° W and 35° N–70° N would eliminate the IVT300 interaction with land.

While most of the IVT300 values along the west coast of Europe during the study period are below 800 kg m^{-1} s^{-1} (Fig. 11a), the values reaching 1400 kg m^{-1} s^{-1} and above in a few instances could lead to extreme ARs. Similarly, the probability density function computed along the same boundary (Fig. 11b) shows the IVT300 could reach up to 1400 kg m^{-1} s^{-1} and cat 1 and cat 2 have a higher probability of occurrence (> 0.01) over Western Europe than other categories.

The study also focuses on the decadal change in frequency of ARs in the North Atlantic (Fig. 12) irrespective of their categories. Thus, ARs show a northward shift in decade 2 (the 1990s–1980s) with positive values in the north and negative in the south (Fig. 12a). This pattern was reversed in decade 3 (the 2000s–1990s) as shown in Fig. 12b. Recent decades show a large increase in the frequency of ARs with strong positives over the north Atlantic (Fig. 12c). The decadal analysis along the 11° W longitude (Fig. 13) shows increasing extreme IVT300 values and their poleward shift in recent decades. All categories show peak frequency between 40° N–60° N and cat 1 ARs frequency has been decreasing along 11° W (Fig. 13a) in the recent decade. Both cat 2 and cat 3 AR events were less frequent (Fig. 13b, c) in the third decade (green). On the other hand, the frequency of cat 3 and cat 4 ARs has been increasing in the last decade (Fig. 13c, d) along 11° W with a poleward movement of ~ 5° towards north and crossing 60° N. The changes in the atmospheric state and the synoptic condition in recent decades could be causing the poleward movement of the intense IVT300. Hence, in the following section, we study the state of the atmosphere during the landfalling of ARs over Western Europe.

3.6 Atmospheric state and synoptic conditions

The Scandinavian blocking including phases of the NAO dominates weather patterns over Europe and Scandinavia through the impact on precipitation and temperature (Madonna et al. 2017). While these patterns are persistent in the North Atlantic-European sector irrespective of the seasons, mostly these patterns control the wintertime weather regimes (Dawson et al. 2012; Hannachi et al. 2017). On the other hand, Western Europe receives more frequent intense ARs in wintertime than in any other season. To study the atmospheric and synoptic conditions while ARs occurrence and landfall along with Western Europe, we study

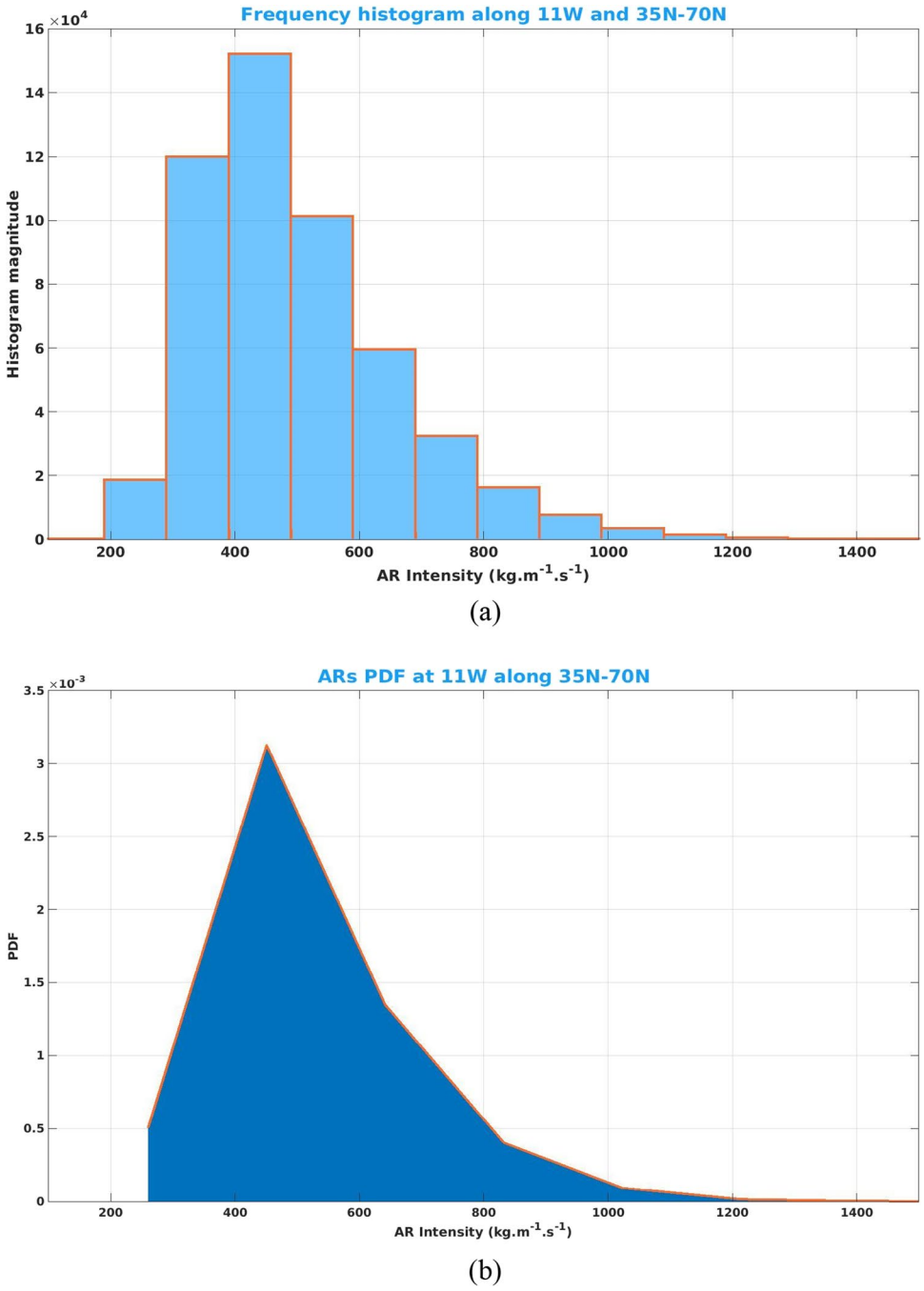

Fig. 11 (**a**) Histogram and (**b**) probability density function of ARs (kg m^{-1} s^{-1}) at 11 W along latitudes 35–70 N

the composite of 500 hPa geopotential (Fig. 14) and surface latent heat flux (Fig. 15) anomalies following Lavers and Villarini (2013b) along 11° W using 5° latitude bins spanning 35° N–70° N (Figure S6). Contrary to Lavers and Villarini (2013b), who used only a few intense ARs, we computed geopotential and surface latent heat flux anomaly composites with all instances (days) where IVT300 was greater than 200 kg m^{-1} s^{-1} in these latitude bins. Initially, we computed this daily geopotential and surface latent heat flux anomalies with respect to the same time (day) period during 1979–2018. Then, these anomalies were picked with respect to the time and location of the occurrence of ARs (IVT300) greater than 200 kg m^{-1} s^{-1} within selected bins and the composite mean anomaly was calculated for each latitude bin.

Geopotential shows a tripole pattern with positive anomalies in the south of the Iberian Peninsula (Fig. 14a, b), Iceland and Greenland, and negative anomalies extend from Britain to the Iberian Peninsula. This is also termed as an Atlantic ridge regime with blocking mainly offshore of the Iberian Peninsula due to Iberian wave breaking (Davini et al. 2014) or southwest European blocking

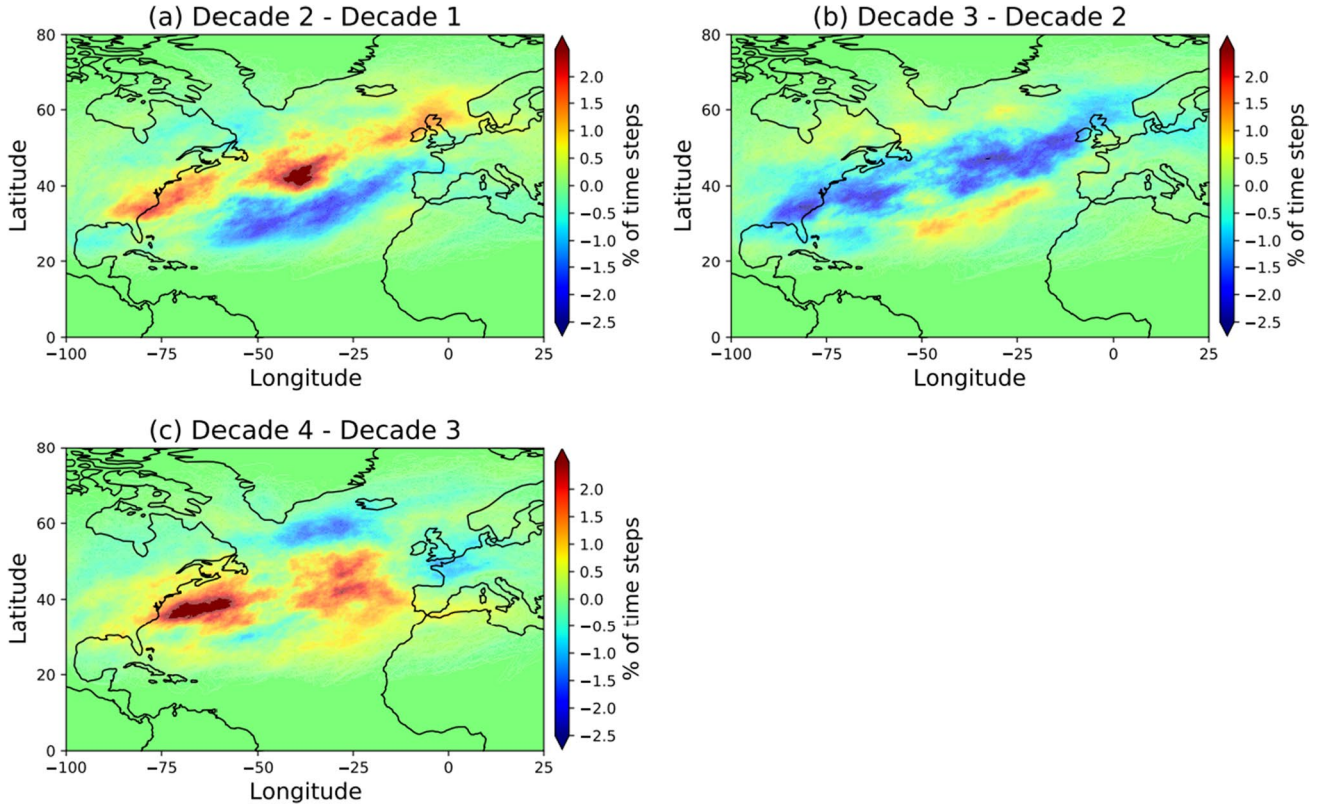

Fig. 12 Decadal changes in frequency of ARs in the North Atlantic

(Woollings et al. 2010) leading to the southward occurring ARs (35° N–45° N). The Greenland anticyclone regime occurs mainly over Greenland resembling the negative phase of the NAO. This negative NAO arrangement would block the flow over northern Europe and the North Atlantic storm track and related heavy precipitation and thus impact southern Europe (Pinto and Raible 2012). The zonal regime with very little blocking resembles the positive phase of the NAO. In a positive NAO phase, negative geopotential anomalies (Fig. 14c, d) in the 45° N–55° N latitude band favors occurrence of frequent ARs within the extratropical cyclones causing rainfall over northern France, through the western British Isles to Norway. A Scandinavian blocking regime is associated with blocking mainly over the European continent and Scandinavia. The occurrence of ARs and their associated precipitation in the north between 55° N and 70° N is related to Scandinavian blocking with the dipole of positive anomalies near the British Isles and negative anomalies over Greenland and Iceland (Fig. 14e–g). Although both NAO and Scandinavian patterns have strong relation with AR occurrence in Europe, it is not obvious that each AR landfall would follow the same synoptic weather patterns as the spatial pattern of the atmospheric state would vary significantly with time over a region.

Southernmost AR events are drawing water vapor from both western and eastern North Atlantic as surface latent heat flux anomalies show a dipole pattern with positive anomalies on either side (Fig. 15a, b). Thus, these regions act as a major source of moisture entraining into ARs and impact the intensity of ARs (IVT300). The north-central Atlantic is the source of moisture for the ARs in the 45° N–55° N latitude band (Fig. 15c, d). Further, a dipole pattern with positive surface latent heat flux anomaly in the west and negative in the east fueling ARs in the far north. Though the positive anomalies over the North Atlantic could lead to intensifying ARs (IVT300) in the north, the cold sea surface and associated negative surface latent heat flux anomalies over the Scandinavia could control the total moisture flux into the ARs and hence the intensity of IVT300 over this region.

4 Conclusions

We study the spatio-temporal variability of water vapor transport (IVT and IWV) and ARs in the Euro-Atlantic basin using six-hourly ERA5 data and evaluated five other reanalysis data sets available from NOAA, NASA, ECMWF, and NCEP during 1979–2018 with ERA5. We use IVT and

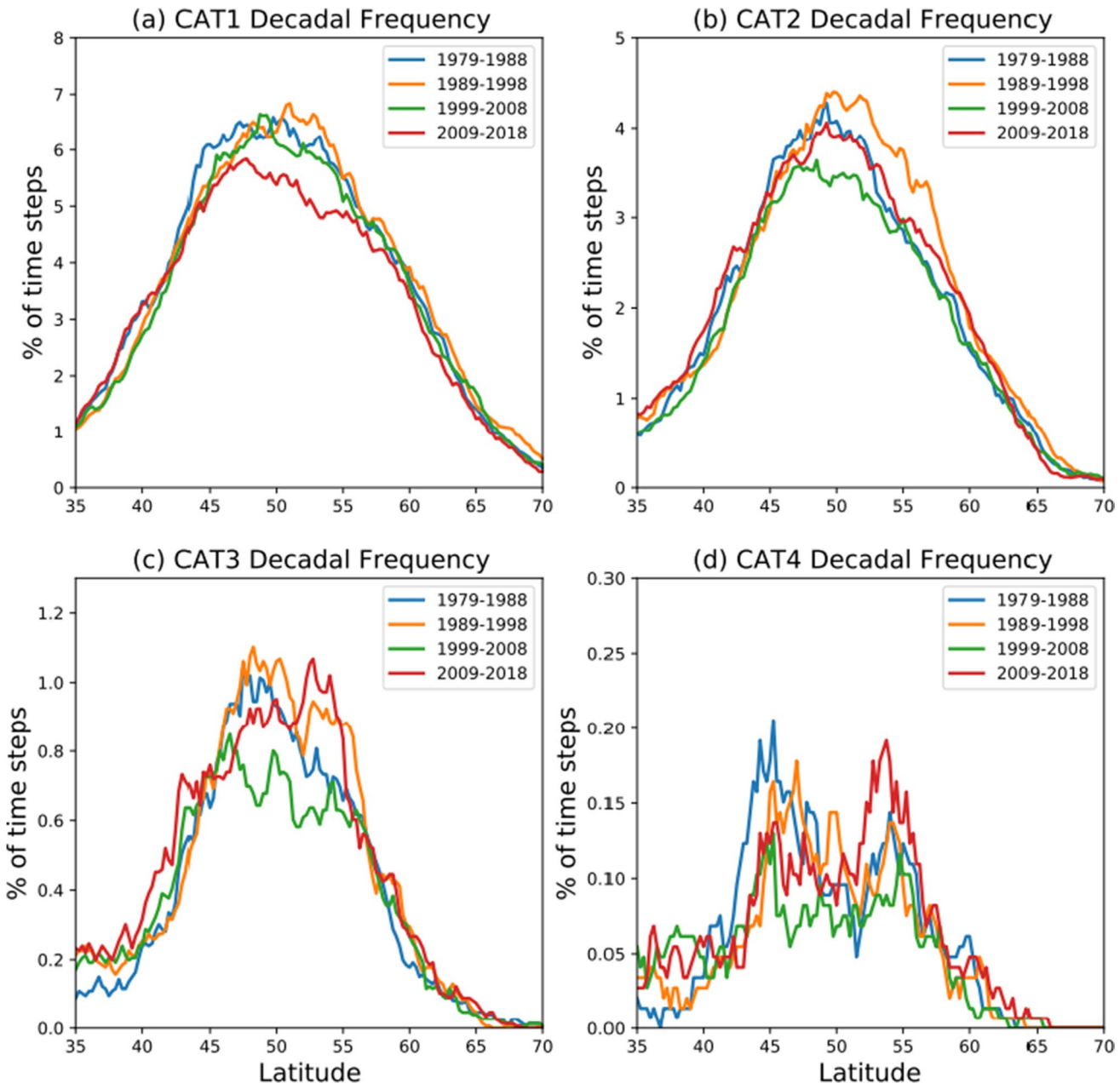

Fig. 13 Frequency of different categories of ARs (kg m^{-1} s^{-1}) along 11° W

IWV methods to map the water vapor transport in different atmospheric layers in the North Atlantic and normalize it with temperature to study the water vapor variability with air temperature. Both IVT and nIVT proved to be accurate enough to map ARs. Though the IVT shows seasonal and semi-annual variability; the mean annual intensity of ARs is ~ 600 kg m^{-1} s^{-1} in the central North Atlantic and the standard deviation is at 33% of the intensity in the North Atlantic. On the other hand, both these values vary in different reanalysis products, with recently released ERA5 showing lower climatology and standard deviation whereas ERA-Interim has higher values compared to other reanalysis datasets. However, the average bias in other datasets is around 50 kg m^{-1} s^{-1} as compared to ERA5 which amounts to ~ 10% of the total observed mean IVT flux in the central North Atlantic. The bias in the magnitude of IVT in different layers is directly proportional to the bias in the Q, U, and V of the respective layers.

Both the accuracy and magnitude of atmospheric variables at different pressure levels (Q, U, and V) in mapping ARs are highly dependent on the resolution of the data obtained. Many of the existing methods and mapping

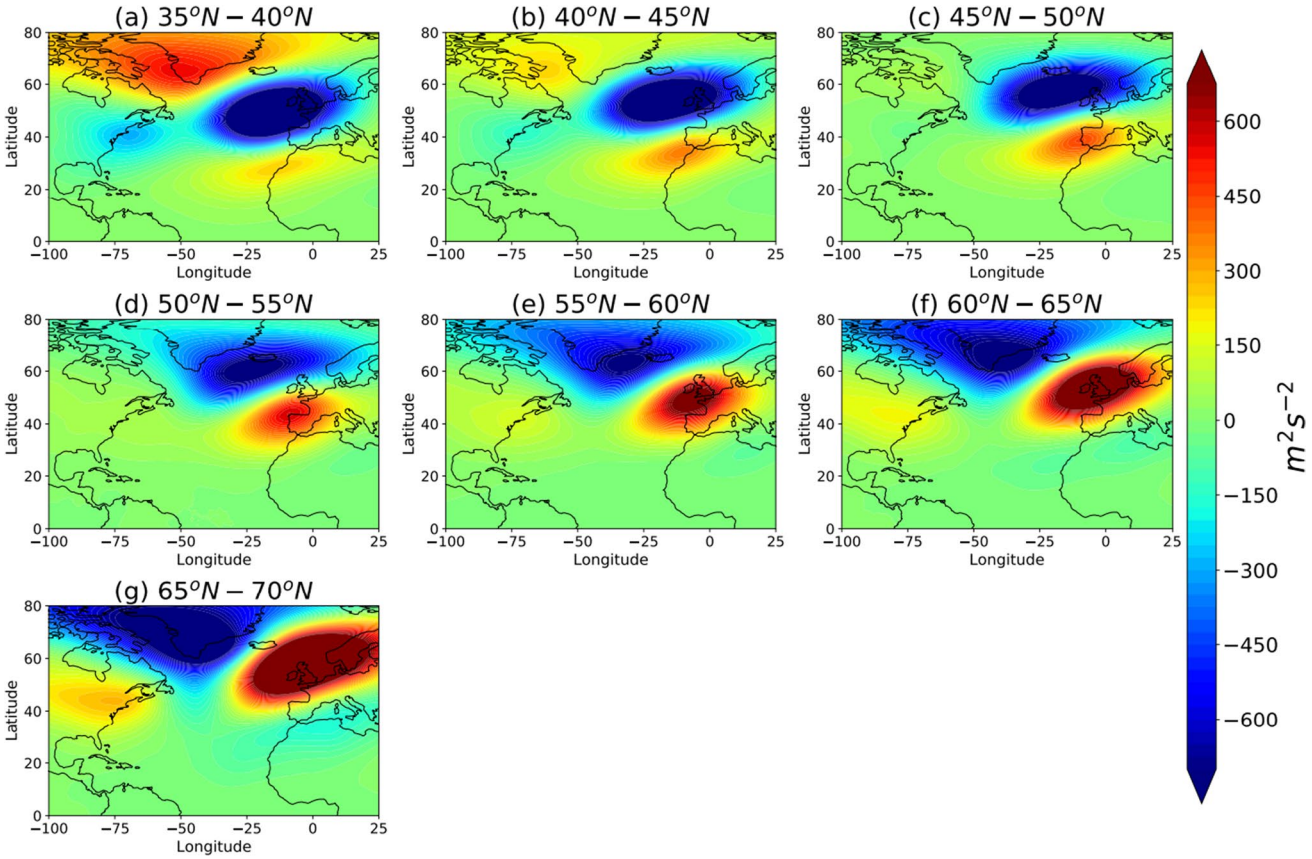

Fig. 14 Composite of geopotential anomaly along 11° W using different bins

techniques are using atmospheric data from satellites and numerical models. Numerical models have limitations in integrating the discretized version of the Navier-Stokes equations. Due to uncertainty in initial conditions, numerical approximation, and model deficiencies, the error increases non-linearly and thus has decreasing forecast skill in simulating the state of the atmosphere with a good lead time (e.g., Lorenz 1963). As the filament structures move with time, and the Eulerian method used to map filaments make it hard to use observations. On the other hand, most of the ARs originate from the large open oceans through both local evaporation and remote moisture flux convergence. Land-based stations could be handy in measuring the atmospheric parameters while the AR approaches to land and landfall. Data obtained from both satellites and statistical methods have limitations in forecasting the landfall and intensity of ARs well in advance. In recent times, machine learning techniques (Chapman et al. 2019; Kashinath et al. 2021) have evolved as other alternatives. However, the mean error in estimating the intensity of ARs through IVT is around 50 kg m^{-1} s^{-1} using different sources of data including data from reanalysis and amounts to 22% of mean observed flux (Chapman et al. 2019; Lavers et al. 2018).

While most of the water vapor flux is located below 500 hPa due to rapidly decreasing saturated moisture flux with height, the upper layer winds are key to the poleward movement of this flux. Hence, the accurate and high-resolution atmospheric parameters at least up to 500 hPa could improve the detection and tracking of ARs in the North Atlantic. On the other hand, the variability and trend of Q, U, and V below 750 hPa guide the strength of the total column IVT. Thus, Q, U, and V below 750 hPa control the magnitude of IVT in the North Atlantic which show an increasing decadal trend with seesaw decadal variability. The IVT and ARs in the North Atlantic show interannual variability with the zonal movement of peak values from the western Atlantic in summer to the eastern Atlantic in winter. However, the summer half-year ARs (IVT) in the North Atlantic show 3% higher intensity than those in the winter half-year with 3% lower intensity as compared to the annual mean due to strong evaporation from the warm ocean in the summer. While the semi-annual spatial trend of IVT300 shows an opposite pattern, the annual trend of IVT300 shows an increasing water vapor flux over the western North Atlantic with a poleward movement of this flux during the last decades. Meanwhile, the IVT300 trend has been increasing

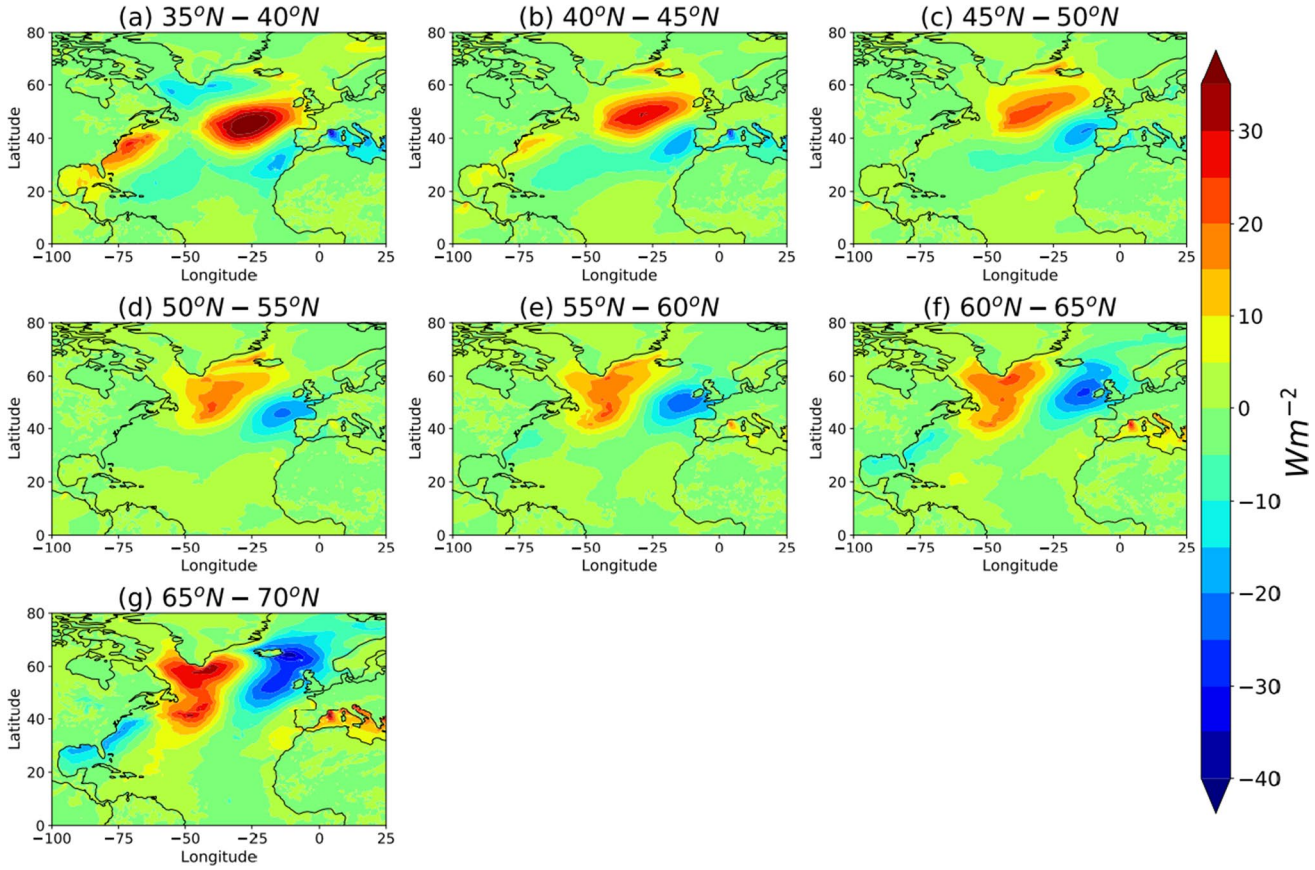

Fig. 15 Composite of surface latent heat flux anomaly along 11° W using different bins

in the recent decades with a strong decadal change in the frequency of ARs over the North Atlantic. Thus, the higher latitudes encountered intense ARs in recent times. Though the cat 1 and cat 2 ARs are more frequent (> 10%) in the North Atlantic, particularly over 40° N–60° N, the rarely occurring (< 5%) cat 3 and cat 4 events could cause extreme precipitation, flooding, and winds over Western Europe. The atmospheric state and synoptic weather guided by Scandinavian blocking and both phases of NAO set the landfall location of ARs along Western Europe.

The impact of climate indices such as El Niño-Southern Oscillation (ENSO), Atlantic multidecadal oscillation, Atlantic zonal mode variability, and changing synoptic circulation patterns on the intensity and frequency of ARs in the North Atlantic and Western Europe need to be explored further to get a better understanding of the characteristics of ARs in this region. Furthermore, the influence of oceanic parameters and the subtropical convection over the source regions in the open oceans, particularly over warm water off the east coast of North America, could lead to the rapid enhancement of IVT in the ARs over this region. Hence, looking at the variability of surface and sub-surface oceanic parameters in the North Atlantic Ocean would be handy to understand the strength of the ARs over this region. Also, changes in the surface temperatures over the Gulf current and subtropical gyre in the North Atlantic Ocean could give more insights on ARs variability in this region. Changes in the coastal sea level and subsurface processes are also key to understand while studying the impacts of the landfalling and poleward shift in ARs. Similarly, the implications of the recent poleward shift in the location of landfalling ARs in the North Atlantic could influence the changes in Greenland and Arctic mass balance.

Finally, the TECA BARD method was tested and applied only to global data. The detector's parameter settings were optimized to match the global AR count. However, the method effectively identifies local peaks in IVT and would technically produce results if applied to a non-global region, with some bias in the AR probabilities (this is untested speculation). Because the North Atlantic region includes the tropics (constant, high IVT) and the poles (constant low IVT) has a good dynamical range in IVT as compared to the global dynamical IVT range, and we assume that method has predicted ARs occurrence satisfactorily.

Supplementary Information The online version contains supplementary material available at https://doi.org/10.1007/s00704-021-03776-w.

Acknowledgements The authors thank NOAA Earth System Research Laboratories (ESRL), the European Centre for Medium-Range Weather Forecasts (ECMWF), the National Aeronautics and Space Administration (NASA), and the National Centers for Environmental Prediction (NCEP) for providing reanalysis datasets. We acknowledge Pyferret software from the NOAA/PMEL. Thanks to Paulo De Luca, Department of Water and Climate Risk, Vrije Universiteit, Amsterdam for useful comments to improve the manuscript. Anonymous reviewers are thanked for critically reading the manuscript and suggesting substantial improvements.

Author contribution Venugopal (as the corresponding author) pursued the idea and analyzed all datasets, results and prepared the draft; Anna and Erik were involved and helped in interpreting and improving both results and the manuscript.

Funding Open access funding provided by Uppsala University. This study was supported by the Department of Earth Sciences, Uppsala University, and the Swedish Research Council (VR) nr 2017–03988.

Data availability All data used in the study are freely available online from the corresponding data sources cited in the article. However, data that support the findings of this study are available on request from the corresponding author.

Code availability All codes used in this study are available on request from the corresponding author.

Declarations

Ethics approval The manuscript has not been submitted to more than one journal for simultaneous consideration. The manuscript has not been published previously (partly or in full) unless the new work concerns an expansion of previous work. Our study is not split up into several parts to increase the number of submissions and submitted to various journals or to one journal over time. No data has been fabricated or manipulated (including images) to support our conclusions. No data or text by others are presented as if they were our own ("plagiarism").

Consent to participate This study does not involve vulnerable groups. We used only meteorological and satellite-based reanalysis data to analyze.

Consent for publication I (Venugopal Thandlam, corresponding author) accept the responsibility for releasing this paper and the materials on behalf of me and all co-authors.

Conflict of interest The authors declare no competing interests.

References

Algarra I, Nieto R, Ramos AM, Eiras-Barca J, Trigo RM, Gimeno L (2020) Significant increase of global anomalous moisture uptake feeding landfalling Atmospheric Rivers. Nat Commun 11(1):1–7

Blamey RC, Ramos AM, Trigo RM, Tomé R, Reason CJC (2018) The influence of atmospheric rivers over the South Atlantic on winter rainfall in South Africa. J Hydrometeorol 19(1):127–142

Champion AJ, Allan RP, Lavers DA (2015) Atmospheric rivers do not explain UK summer extreme rainfall. J Geophys Res Atmos 120(14):6731–6741

Chapman WE, Subramanian AC, Delle Monache L, Xie SP, Ralph FM (2019) Improving atmospheric river forecasts with machine learning. Geophys Res Lett 46(17–18):10627–10635

Cheng BS, Chang AL, Deck A, Ferner MC (2016) Atmospheric rivers and the mass mortality of wild oysters: insight into an extreme future? Proc R Soc B Biol Sci 283(1844):20161462

Compo, G. P., Whitaker, J. S., Sardeshmukh, P. D., Matsui, N., Allan, R. J., Yin, X., ... & Worley, S. J. (2011). The twentieth century reanalysis project. Quarterly Journal of the Royal Meteorological Society, 137(654), 1-28

Cordeira JM, Stock J, Dettinger MD, Young AM, Kalansky JF, Ralph FM (2019) A 142-year climatology of northern California landslides and atmospheric rivers. Bull Am Meteor Soc 100(8):1499–1509

Davini P, Cagnazzo C, Fogli PG, Manzini E, Gualdi S, Navarra A (2014) European blocking and Atlantic jet stream variability in the NCEP/NCAR reanalysis and the CMCC-CMS climate model. Climate Dynamics 43(1–2):71–85

Dawson A, Palmer TN, Corti S (2012) Simulating regime structures in weather and climate prediction models. Geophysical Research Letters, 39(21)

De Luca P, Hillier JK, Wilby RL, Quinn NW, Harrigan S (2017) Extreme multi-basin flooding linked with extra-tropical cyclones. Environ Res Lett 12(11):114009

Dee, D. P., Uppala, S. M., Simmons, A. J., Berrisford, P., Poli, P., Kobayashi, S., ... & Vitart, F. (2011). The ERA-Interim reanalysis: configuration and performance of the data assimilation system. Quarterly Journal of the royal meteorological society, 137(656), 553-597.

Dettinger M (2011) Climate change, atmospheric rivers, and floods in California–a multimodel analysis of storm frequency and magnitude changes 1. JAWRA J Am Water Resour Assoc 47(3):514–523

Dettinger MD, Ralph FM, Das T, Neiman PJ, Cayan DR (2011) Atmospheric rivers, floods and the water resources of California. Water 3:445–478

Espinoza V, Waliser DE, Guan B, Lavers DA, Ralph FM (2018) Global analysis of climate change projection effects on atmospheric rivers. Geophys Res Lett 45(9):4299–4308

Fish MA, Wilson AM, Ralph FM (2019) Atmospheric river families: definition and associated synoptic conditions. J Hydrometeorol 20(10):2091–2108

Florsheim JL, Dettinger MD (2015) Promoting atmospheric-river and snowmelt-fueled biogeomorphic processes by restoring river-floodplain connectivity in California's Central Valley. In Geomorphic approaches to integrated floodplain management of lowland fluvial systems in North America and Europe (pp. 119–141). Springer, New York, NY

Stohl A, Forster C, Sodemann H (2008) Remote sources of water vapor forming precipitation on the Norwegian west coast at 60 N–a tale of hurricanes and an atmospheric river. J Geophys Res Atmos 113(D5)

Gao Y, Lu J, Leung LR (2016) Uncertainties in projecting future changes in atmospheric rivers and their impacts on heavy precipitation over Europe. J Clim 29(18):6711–6726

Gelaro, R., McCarty, W., Suárez, M. J., Todling, R., Molod, A., Takacs, L., ... & Zhao, B. (2017). The modern-era retrospective analysis for research and applications, version 2 (MERRA-2). Journal of climate, 30(14), 5419-5454

Gimeno L, Stohl A, Trigo RM, Dominguez F, Yoshimura K, Yu L, ... Nieto R (2012) Oceanic and terrestrial sources of continental precipitation. Rev Geophys 50(4)

Gimeno L, Nieto R, Vázquez M, Lavers DA (2014) Atmospheric rivers: a mini-review. Front Earth Sci 2:2

Gimeno L (2013) Grand challenges in atmospheric science. Front Earth Sci 1:1

Gonzales KR, Swain DL, Nardi KM, Barnes EA, Diffenbaugh NS (2019) Recent warming of landfalling atmospheric rivers along the west coast of the United States. J Geophys Res Atmos 124(13):6810–6826

Gorodetskaya IV, Tsukernik M, Claes K, Ralph MF, Neff WD, Van Lipzig NP (2014) The role of atmospheric rivers in anomalous snow accumulation in East Antarctica. Geophys Res Lett 41(17):6199–6206

Guan B, Waliser DE (2017) Atmospheric rivers in 20 year weather and climate simulations: a multimodel, global evaluation. J Geophys Res Atmos 122(11):5556–5581

Guan B, Waliser DE (2015) Detection of atmospheric rivers: evaluation and application of an algorithm for global studies. J Geophys Res Atmos 120(24):12514–12535

Guan B, Molotch NP, Waliser DE, Fetzer EJ, Neiman PJ (2010) Extreme snowfall events linked to atmospheric rivers and surface air temperature via satellite measurements. Geophys Res Lett 37(20)

Hack JJ, Caron JM, Yeager SG, Oleson KW, Holland MM, Truesdale JE, Rasch PJ (2006) Simulation of the global hydrological cycle in the CCSM Community Atmosphere Model version 3 (CAM3): Mean features. J Clim 19(11):2199–2221

Hannachi A, Straus DM, Franzke CL, Corti S, Woollings T (2017) Low-frequency nonlinearity and regime behavior in the Northern Hemisphere extratropical atmosphere. Rev Geophys 55(1):199–234

Hersbach H, Bell B, Berrisford P, Hirahara S, Horányi A, Muñoz-Sabater J, ... Schepers D (2017) Complete ERA5: Fifth Generation of ECMWF Atmospheric Reanalyses of the Global Climate. Copernicus Climate Change Service (C3S) Data Store (CDS)

Jiang T, Deng Y (2011) Downstream modulation of North Pacific atmospheric river activity by East Asian cold surges. Geophys Res Lett 38(20)

Kamae Y, Mei W, Xie SP (2017) Climatological relationship between warm season atmospheric rivers and heavy rainfall over East Asia. Journal of the Meteorological Society of Japan. Ser. II

Kanamitsu M, Ebisuzaki W, Woollen J, Yang SK, Hnilo JJ, Fiorino M, Potter GL (2002) Ncep–doe amip-ii reanalysis (r-2). Bull Am Meteor Soc 83(11):1631–1644

Kashinath K, Mudigonda M, Kim S, Kapp-Schwoerer L, Graubner A, Karaismailoglu E, ... Collins W (2021) ClimateNet: an expert-labeled open dataset and deep learning architecture for enabling high-precision analyses of extreme weather. Geoscientific Model Development, 14(1), 107-124

Brubaker KL, Dara Entekhabi, Peter S. Eagleson. Atmospheric water vapor transport and continental hydrology over the Americas. Tech Rep 3–4, 1994

Khouakhi A, Villarini G (2016) On the relationship between atmospheric rivers and high sea water levels along the US West Coast. Geophys Res Lett 43(16):8815–8822

Komatsu KK, Alexeev VA, Repina IA, Tachibana Y (2018) Poleward upgliding Siberian atmospheric rivers over sea ice heat up Arctic upper air. Sci Rep 8(1):1–15

Kundzewicz ZW, Radziejewski M, Pinskwar I (2006) Precipitation extremes in the changing climate of Europe. Climate Res 31(1):51–58

Lavers DA, Villarini G (2013a) Atmospheric rivers and flooding over the central United States. J Clim 26(20):7829–7836

Lavers DA, Villarini G (2013b) The nexus between atmospheric rivers and extreme precipitation across Europe. Geophys Res Lett 40(12):3259–3264

Lavers DA, Villarini G (2015) The contribution of atmospheric rivers to precipitation in Europe and the United States. J Hydrol 522:382–390

Lavers DA, Pappenberger F, Richardson DS, Zsoter E (2016) ECMWF Extreme Forecast Index for water vapor transport: a forecast tool for atmospheric rivers and extreme precipitation. Geophys Res Lett 43(22):11–852

Lavers DA, Villarini G, Allan RP, Wood EF, Wade AJ (2012) The detection of atmospheric rivers in atmospheric reanalyses and their links to British winter floods and the large-scale climatic circulation. J Geophys Res Atmos 117(D20)

Lavers, D. A., Rodwell, M. J., Richardson, D. S., Ralph, F. M., Doyle, J. D., Reynolds, C. A., ... & Pappenberger, F. (2018). The gauging and modeling of rivers in the sky. Geophys Res Lett 45(15), 7828-7834

Lavers DA, Allan RP, Wood EF, Villarini G, Brayshaw DJ, Wade AJ (2011) Winter floods in Britain are connected to atmospheric rivers. Geophys Res Lett 38(23)

Leung LR, Qian Y (2009) Atmospheric rivers induced heavy precipitation and flooding in the western US simulated by the WRF regional climate model. Geophys Res Lett 36(3)

Lorenz EN (1963) Deterministic nonperiodic flow. J Atmos Sci 20:130–141

Madonna E, Li C, Grams CM, Woollings T (2017) The link between eddy-driven jet variability and weather regimes in the North Atlantic-European sector. Q J R Meteorol Soc 143(708):2960–2972

Mattingly KS, Mote TL, Fettweis X (2018) Atmospheric river impacts on Greenland Ice Sheet surface mass balance. J Geophys Res Atmos 123(16):8538–8560

Millán MM (2014) Extreme hydrometeorological events and climate change predictions in Europe. J Hydrol 518:206–224

Nash D, Waliser D, Guan B, Ye H, Ralph FM (2018) The role of atmospheric rivers in extratropical and polar hydroclimate. J Geophys Res Atmos 123(13):6804–6821

Neff W (2018) Atmospheric rivers melt Greenland. Nat Clim Chang 8(10):857–858

Neiman PJ, Ralph FM, White AB, Kingsmill DE, Persson POG (2002) The statistical relationship between upslope flow and rainfall in California's coastal mountains: Observations during CALJET. Mon Weather Rev 130(6):1468–1492

Neiman PJ, Ralph FM, Wick GA, Lundquist JD, Dettinger MD (2008a) Meteorological characteristics and overland precipitation impacts of atmospheric rivers affecting the West Coast of North America based on eight years of SSM/I satellite observations. J Hydrometeorol 9(1):22–47

Neiman PJ, Ralph FM, Wick GA, Kuo YH, Wee TK, Ma Z., ... Dettinger MD (2008b) Diagnosis of an intense atmospheric river impacting the Pacific Northwest: Storm summary and offshore vertical structure observed with COSMIC satellite retrievals. Mon Weather Rev 136(11):4398–4420. https://doi.org/10.1007/s00704-021-03776-w

Neiman PJ, White AB, Ralph FM, Gottas DJ, Gutman SI (2009) A water vapour flux tool for precipitation forecasting. In: Proceedings of the institution of civil engineers-water management (Vol. 162, No. 2, pp. 83–94). Thomas Telford Ltd.

Neiman PJ, Schick LJ, Ralph FM, Hughes M, Wick GA (2011) Flooding in western Washington: the connection to atmospheric rivers. J Hydrometeorol 12(6):1337–1358

O'Brien TA, Risser MD, Loring B, Elbashandy AA, Krishnan H, Johnson J, ... Collins WD (2020) Detection of atmospheric rivers with inline uncertainty quantification: TECA-BARD v1. 0.1. Geoscientific Model Development, 13(12), 6131–6148

Pasquier JT, Pfahl S, Grams CM (2019) Modulation of atmospheric river occurrence and associated precipitation extremes in the North Atlantic region by European weather regimes. Geophys Res Lett 46(2):1014–1023

Payne AE, Demory ME, Leung LR, Ramos AM, Shields CA, Rutz JJ, ... Ralph FM (2020) Responses and impacts of atmospheric rivers to climate change. Nat Rev Earth Environ 1(3), 143-157

Pinto JG, Raible CC (2012) Past and recent changes in the North Atlantic oscillation. Wiley Interdiscip Rev Clim Change 3(1):79–90

Pinto JG, Bellenbaum N, Karremann MK, Della-Marta PM (2013) Serial clustering of extratropical cyclones over the North Atlantic and Europe under recent and future climate conditions. J Geophysl Res Atmos 118(22):12–476

Ralph FM, Neiman PJ, Wick GA (2004) Satellite and CALJET aircraft observations of atmospheric rivers over the eastern North Pacific Ocean during the winter of 1997/98. Mon Weather Rev 132(7):1721–1745

Ralph FM, Neiman PJ, Rotunno R (2005) Dropsonde observations in low-level jets over the northeastern Pacific Ocean from CALJET-1998 and PACJET-2001: Mean vertical-profile and atmospheric-river characteristics. Mon Weather Rev 133(4):889–910

Ralph FM, Dettinger MD (2011) Storms, floods, and the science of atmospheric rivers. EOS Trans Am Geophys Union 92(32):265–266

Ralph FM, Neiman PJ, Wick GA, Gutman SI, Dettinger MD, Cayan DR, White AB (2006) Flooding on California's Russian River: Role of atmospheric rivers. Geophys Res Lett 33(13)

Ralph FM, Rutz JJ, Cordeira JM, Dettinger M, Anderson M, Reynolds D, ... Smallcomb C (2019) A scale to characterize the strength and impacts of atmospheric rivers. Bull Am Meteorol Soc 100(2): 269-289

Ramos AM, Blamey RC, Algarra I, Nieto R, Gimeno L, Tomé R, ... Trigo RM (2018) From Amazonia to southern Africa: atmospheric moisture transport through low-level jets and atmospheric rivers. Ann. NY Acad. Sci 1436: 217-230

Roberge A, Gyakum JR, Atallah EH (2009) Analysis of intense poleward water vapor transports into high latitudes of western North America. Weather Forecast 24(6):1732–1747

Saha S, Moorthi S, Wu X, Wang J, Nadiga S, Tripp P, ... Becker E (2014) The NCEP climate forecast system version 2. Journal of climate, 27(6), 2185-2208

Schneider EK, Kirtman BP, Lindzen RS (1999) Tropospheric water vapor and climate sensitivity. J Atmos Sci 56(11):1649–1658

Shields CA, Rutz JJ, Leung LY, Ralph FM, Wehner M, Kawzenuk B, Nguyen P (2018) Atmospheric river tracking method intercomparison project (ARTMIP): project goals and experimental design. Geosci Model Dev 11(6):2455–2474

Sellars SL, Kawzenuk B, Nguyen P, Ralph FM, Sorooshian S (2017) Genesis, pathways, and terminations of intense global water vapor transport in association with large-scale climate patterns. Geophys Res Lett 44(24):12–465

Sodemann H, Stohl A (2013) Moisture origin and meridional transport in atmospheric rivers and their association with multiple cyclones. Mon Weather Rev 141(8):2850–2868

Thapa K (2015) Atmospheric rivers carry non-monsoon extreme precipitation into western Nepal. State University of New York College of Environmental Science and Forestry

Trenberth KE (2011) Changes in precipitation with climate change. Climate Res 47(1–2):123–138

Van den Besselaar EJM, Klein Tank AMG, Buishand TA (2013) Trends in European precipitation extremes over 1951–2010. Int J Climatol 33(12):2682–2689

Viale M, Nuñez MN (2011) Climatology of winter orographic precipitation over the subtropical central Andes and associated synoptic and regional characteristics. J Hydrometeorol 12(4):481–507

Waliser D, Guan B (2017) Extreme winds and precipitation during landfall of atmospheric rivers. Nat Geosci 10(3):179–183

Woollings T, Hannachi A, Hoskins B (2010) Variability of the North Atlantic eddy-driven jet stream. Q J R Meteorol Soc 136(649):856–868

Yang Y, Zhao T, Ni G, Sun T (2018) Atmospheric rivers over the Bay of Bengal lead to northern Indian extreme rainfall. Int J Climatol 38(2):1010–1021

Zhu Y, Newell RE (1998) A proposed algorithm for moisture fluxes from atmospheric rivers. Mon Weather Rev 126(3):725–735

Zhu Y, Newell RE (1994) Atmospheric rivers and bombs. Geophys Res Lett 21(18):1999–2002